Laminar shallow viscoplastic fluid flowing through an array of vertical obstacles

Noé Bernabeu, Pierre Saramito, Andrew Harris

Laminar shallow viscoplastic fluid flowing through an array of vertical obstacles

Noé Bernabeu, Pierre Saramito, Andrew Harris

November 23, 2017

Abstract – A new Bingham-Darcy shallow depth approximation flow model is proposed in this paper. This model is suitable for a laminar shallow viscoplastic fluid flowing on a general topography and crossing an array of vertical obstacles. An analogous porous medium is first introduced for reducing the array of obstacles. It bases on a continuum model similar to the Brinkman equations, where the usual Darcy model is extended for viscoplastic Bingham fluids. Next, a specific asymptotic analysis of this Bingham-Darcy porous medium in the case of shallow depth flows leads to a new reduced model. The resulting highly nonlinear parabolic equation in terms of the flow height only is efficiently solved by a Newton method, without any regularization. The numerical predictions compares both qualitatively and quantitatively well with both some experimental measurements and full tridimensional simulations. Finally, a new experiment for a viscoplastic flow over an inclined plane through a network of obstacle is proposed and numerical simulations are provided for future comparisons with experiments.

1 Introduction

The problem of complex fluids flowing through networks of discrete obstacles applies to many applications in natural and material sciences. During natural risk assessments, for example, volcanic debris and/or lava flows may move through dense forests, as was the case for lavas advancing during Kilauea's July 1974 eruption [24] and Etna's 2002-03 eruption [2], among others. To date, lava flow emplacement models have tended to consider tree-free surfaces in completing their simulations (e.g., [6, 18, 20]). The same applies to non-volcanic debris flows in forested mountainous or urban areas (see e.g. [15, 31]). In terms of material sciences, flow of a viscoplastic fluid through arrays of solid cylinders needs to be considered in industrial processes such as the case of fresh concrete spreading through networks of steel bars (see e.g. [40, 41]).

Taking into account each obstacle in numerical simulations leads to very time consuming computations. The usual approach is to replace the discrete configuration of obstacles by an equivalent continuous medium, the so-called fibrous porous medium. In the case of a

Newtonian fluid, this continuous medium is described by the classical Darcy model [14]. This model proposes a linear relation between the flow rate and the pressure drop across the porous medium. In 1949, Brinkman [12] proposed a modification of the classical Darcy model by combining the Navier-Stokes equations with the Darcy model. This combination is useful for situations where there is both flow sub-regions with and without porous media. The Brinkman model provides a global description of both these sub-regions, while the Darcy model alone was unable to describe regions without porous media. Conversely, in the case of a non-Newtonian fluid, the situation is rather complex, due to, from one hand, the complexity of the fluid behavior, and from the other hand, due to the porous micro-structure. Bourgeat and Mikelić [10] proposed a first theoretical analysis of of quasi-Newtonian shear-thinning and shear-thickening fluids and derived a modified Darcy model. This modified Darcy model involves an effective viscosity η_{eff}, which depends both upon the flow rate and the microstructural characteristics of the porous medium: the permeability tensor $\boldsymbol{\kappa}$ and porosity ϕ. The porosity ϕ interprets as the volume fraction of fluid in the medium constituted by both the fluid and the obstacles: it is equal to one for a medium without obstacles and tends to zero when the obstacle density increases. The permeability $\boldsymbol{\kappa}$ depends both upon ϕ and the geometric configuration of the obstacles: some explicit expressions of $\boldsymbol{\kappa}$ vs ϕ exists, depending on the geometrical hypothesis upon the obstacles distribution. For Non-Newtonian viscoplastic fluids, a yield stress have to be reached for obtaining a transition between the unyielded, arrested, state and the yielded state (see e.g. [34, 35]). Thus, there fluids do not typically obey to the usual linear Darcy model in their rheological response to an applied stress, as there is also some no-flow situations in porosities [19, 32]. Pascal [28], based on an experimental investigation, proposed for an Herschel-Bulkley viscoplastic fluid a modified Darcy model that uses a threshold gradient. Some papers focused on the specific flow through packed beds of spherical particles. Al-Fariss and Pinder [1] extended the Pascal's model by deriving an equation for the threshold gradient to describe the flow of waxy oil through beds of packed spheres. Chevalier et al. [13], based on experimental measurements with an yield stress fluid through packed glass beads, proposed an empirical relationship between the pressure drop and the flow rate. Recent studies consider complex fluids flow through fibrous porous media. Bleyer and Coussot [8] performed two-dimensional numerical simulations of a viscoplastic flow through an ordered array of disks and proposed a quite general modified Darcy model of these fluids. Shahsavari and McKinley [36] investigated the flow of yield stress fluids through fibrous media by means of numerical studies and a scaling analysis. They developed an effective viscosity function which can be used in the modified Darcy model for steady fully-developed viscoplastic flows. Vasilic et al. [40] defined an apparent shear rate using a shift factor and a generalized Brinkman equation. Their also performed some numerical simulations using a bi-viscosity regularized viscoplastic model and compared with experimental measurements on a Carbopol gel flow which was slowly poured into a transparent container where an array of cylindrical steel is located in the middle zone. Comparing simulations and experimental observations, They obtained both qualitative and quantitative agreements for the final shape of the flow, at the arrested state.

For thin flows, an usual approach is to consider shallow-depth approximations. The shallow-flow approximations of laminar viscoplastic Bingham fluids were first studied by Liu and Mei [25], based on a rigorous asymptotic analysis. This approach was revisited

by Balmforth and Craster [4] and extended to the axisymmetric case [3], with application to volcanic lava domes. For fast flows, such as debris and mud flows on mountain slopes, Laigle and Coussot derived in [23] the first reduced model that combines both inertia and viscoplastic effects. Viscoplastic effects are estimated from the friction at the bottom. Assuming a compressible material, Bresch et al. derived in [11] a reduced viscoplastic model that also includes inertia effects. This approach was next revisited in the incompressible case in terms of asymptotic analysis by Fernández-Nieto et al. in [16] and by Ionescu in [21] with an augmented Lagrangian algorithm. Practical predictions of natural hazard require to take into account general tridimensional and complex topographies (see e.g. [5]). A new approach for topography in shallow flow models was proposed by Bouchut et al. in [9] which relaxes most restrictions, such as slowly varying topographies. Next, Ionescu in [22], considering Bingham and Drucker-Prager models, extended this approach with an elegant formulation based on surface differential operators (surface gradient and divergence) and also included inertia effects. For a more exhaustive review about various shallow flow approximations of viscoplastic fluids, see the recent review paper [35].

The present model proposes for the first time a shallow-flow approximation of both the Bingham-Brickman model, involving a modified Darcy model for viscoplastic fluids. This model is of practical interest to assess risks, by opening the possibility to numerically investigate the effects of forests on the spatial and temporal flow propagation. This model could be also useful for industrial processes, such as fresh concrete spreading through arrays of steel bars, as the required computing time is dramatically decreased. Instead of time-dependent tridimensional simulations with moving free-surfaces, the present model requires only the resolution a simple two-dimensional parabolic equation for the flow height. The array of obstacles is first reduces to a continuum model by a generalized tensor Brinkman equations for yield stress fluids. Second, assuming a shallow flow, we extends a previous asymptotic analysis [5] to the Brinkman equations extended for the Bingham model.

An outline of the paper is as follows. Section 2 proposes a new shallow-depth approximation of the viscoplastic Bingham model flowing on a general topography and crossing an arrays of vertical obstacles. Section 3 proposes a Newton algorithm for efficiently solve the unregularized nonlinear Bingham-Brickman reduced model. Comparisons between numerical simulations and experimental observations are presented and discussed in section 4. Finally, the flow of viscoplastic fluids on an inclined plane through different fibrous mediums is numerically investigated, in order to understand and quantify the influence of the obstacles on the flow propagation. This numerical experiment could be reproduced with real fluids for future comparisons and benchmarking. The impatient reader, who is not involved by the asymptotic analysis, can read paragraph 2.1 for the initial problem, then paragraph 2.5 for the final reduced one and finally jump to section 4 for results and discussion.

2 Bingham-Darcy shallow depth approximation

2.1 The initial tridimensional problem

We consider the Bingham model [7] constitutive equation which expresses the deviatoric part $\boldsymbol{\tau}$ of the stress tensor versus the rate of deformation tensor $\dot{\boldsymbol{\gamma}}$ as:

$$\begin{cases} \boldsymbol{\tau} = \eta\dot{\boldsymbol{\gamma}} + \tau_y \frac{\dot{\boldsymbol{\gamma}}}{|\dot{\boldsymbol{\gamma}}|} & \text{when } \dot{\boldsymbol{\gamma}} \neq 0, \\ |\boldsymbol{\tau}| \leqslant \tau_y & \text{otherwise.} \end{cases} \tag{1}$$

where $\eta > 0$ is the plastic viscosity and $\tau_y \geqslant 0$ is the yield stress. Here $|\boldsymbol{\tau}| = ((1/2)\sum_{i,j=1}^{3} \tau_{ij}^2)^{1/2}$ denotes the conventional norm of a symmetric tensor in mechanics. The total Cauchy stress tensor is $\boldsymbol{\sigma} = -p.\mathbf{I} + \boldsymbol{\tau}$ where p is the pressure and $\mathbf{I}$ the identity tensor. We suppose that the array of obstacles can be treated as an equivalent continuum porous medium. The constitutive equation (1) is then completed by the conservations of momentum and mass:

$$\rho\left(\partial_t \mathbf{u} + (\mathbf{u}.\boldsymbol{\nabla})\mathbf{u}\right) - \mathbf{div}(\boldsymbol{\tau}) + \boldsymbol{\nabla} p = \mathbf{f}_p + \rho\mathbf{g}, \tag{2}$$

$$\operatorname{div} \mathbf{u} = 0, \tag{3}$$

where $\rho > 0$ is the constant density, $\mathbf{g}$ is the gravity vector and $\mathbf{f}_p$ a source term based on local generalized Darcy's law (e.g. see [29]) relating the force exerced on the pore fluid (typically gradient pressure and gravity force) to the macroscopic-scale velocity by:

$$\mathbf{f}_p = -\eta_{\text{eff}} \boldsymbol{\kappa}^{-1} \mathbf{u}, \tag{4}$$

where $\eta_{\text{eff}} \geqslant 0$ is the material local apparent viscosity and $\boldsymbol{\kappa}$ the permeability tensor. The conservation equations with the addition of a Darcy source term in momentum equation is called Brinkmann equations [12]. This model allows to deal with a mixed cases where only a part of the calculation domain is taken up by a fibrous porous medium. In this case, out of the porous zone, the permeability is infinite and the source term $\mathbf{f}_p$ is vanished that gives the standard conservation equations.
It proved in [27, 30] that the permeability tensor is symmetric and positive definite. That means that the permeability tensor has three principal orthogonal axes and three positive principal values. For an arbitrary porous medium, it is possible to find a coordinate system (x, y, z) in which the permeability tensor has the diagonal form. When the medium is anisotropic, at least two elements of the diagonalized permeability tensor are not equal. Otherwise, when it does not depend on direction, then the permeability is isotropic, and the elements of the diagonalized permeability tensor are equal. If the distribution of pores or principal directions varies from one point in the medium to another, the permeability tensor is spacially heterogeneous, otherwise, it is homogeneous.

In our case with an array of vertical obstacles, the equivalent continuum medium is a fibrous porous one. For convenience, we assume that the z-axis is parallel to the fibers axis and that the arrangement of fibers is uniform in each direction perpendicular to the z-axis, so $\boldsymbol{\kappa} = \operatorname{diag}(\kappa_{\parallel}, \kappa_{\parallel}, \kappa_{\perp})$, where $\kappa_{\parallel}$ is the permeability in the direction perpendicular to the fibers and $\kappa_{\perp}$ the permeability in the direction parallel to the fibers. The local strain

rate is a complex function of the geometry and the fiber arrangement. In the equivalent porous media, it is necessary to define a local effective shear rate $\dot{\boldsymbol{\gamma}}_{\text{eff}}$ which is for the fibrous media a diagonal tensor where its components are frequently expressed [37]:

$$\dot{\gamma}_{\text{eff},ii} = \frac{\alpha_{ii}\mathbf{u}_i}{\sqrt{\kappa_{ii}\phi}}, \ \forall i \in \{x, y, z\},$$

where $\boldsymbol{\alpha} = \text{diag}(\alpha_{ii})_{i\in\{x,y,z\}}$ denotes the medium dependent *shift factor* (also called the *shape factor*) and α_{ii} is factor in the principal direction i. Different expressions are proposed in [36, 41] for viscoplastic fluids. We assume that $\boldsymbol{\alpha}$ has the same form as the permeability tensor: $\boldsymbol{\alpha} = \text{diag}(\alpha_{\parallel}, \alpha_{\parallel}, \alpha_{\perp})$. Let us introduce the tensor $\boldsymbol{A} = \text{diag}(\alpha_{\parallel}/\sqrt{\kappa_{\parallel}\phi}, \alpha_{\parallel}/\sqrt{\kappa_{\parallel}\phi}, \alpha_{\perp}/\sqrt{\kappa_{\perp}\phi})$. When $\dot{\boldsymbol{\gamma}}_{\text{eff}} \neq 0$, which is equivalent to $\mathbf{u} \neq \mathbf{0}$, from the Bingham constitutive equation (1), we obtain the following expression of the effective viscosity:

$$\begin{aligned}\eta_{\text{eff}}(\dot{\boldsymbol{\gamma}}_{\text{eff}}) &= \eta + \frac{\tau_y}{|\dot{\boldsymbol{\gamma}}_{\text{eff}}|} \\ &= \eta + \frac{\tau_y}{|\boldsymbol{A}\mathbf{u}|},\end{aligned}$$

which when combined with the generalized Darcy's law leads when $\mathbf{u} \neq \mathbf{0}$ to the following expression

$$\mathbf{f}_p = -\left(\frac{\tau_y}{|\boldsymbol{A}\mathbf{u}|} + \eta\right)\boldsymbol{\kappa}^{-1}\mathbf{u}.$$

In the general case, we obtain a tensor generalization of the Pascal's law [28] for an anisotropic fibrous media:

$$\begin{cases} \mathbf{f}_p = -\left(\dfrac{\tau_y}{|\boldsymbol{A}\mathbf{u}|} + \eta\right)\boldsymbol{\kappa}^{-1}\mathbf{u}, & \text{when } \mathbf{u} \neq \mathbf{0}, \\ |\boldsymbol{A}\boldsymbol{\kappa}\mathbf{f}_p| \leqslant \tau_y & \text{when } \mathbf{u} = \mathbf{0}. \end{cases} \tag{5}$$

The yield stress τ_y leads to a threshold condition for the transition between "solid" and "fluid" rheological behaviour inside the porous zone in term of the anisotropic norm $|\boldsymbol{A}\boldsymbol{\kappa}\cdot|$. There are five equations (1)-(5) and four unknowns $\boldsymbol{\tau}$, $\mathbf{u}, p$ and $\mathbf{f}_p$.

We consider a flow over a variable topograhy as supplied from a vent and passing through a porous zone (see Fig. 1). For any time $t > 0$, the flow domain is represented by:

$$\Lambda(t) = \{(x, y, z) \in \Omega \times \mathbb{R};\ f(x, y) < z < f(x, y) + h(t, x, y)\}$$

where Ω is an open and bounded subset of $\mathbb{R}^2$. The function f denotes the topography and h the flow height. The boundary $\partial\Lambda(t)$ of the flow volume $\Lambda(t)$ can be split into three parts (see Fig. 1): the basal topography Γ_s, the flow (upper) free surface $\Gamma_f(t)$, and the lateral part $\Gamma_w(t)$, defined by:

$$\begin{aligned}\Gamma_s &= \{(x, y, z) \in \Omega \times \mathbb{R};\ z = f(x, y)\} \\ \Gamma_f(t) &= \{(x, y, z) \in \Omega \times \mathbb{R};\ z = f(x, y) + h(t, x, y)\} \\ \Gamma_w(t) &= \{(x, y, z) \in \partial\Omega \times \mathbb{R};\ f(x, y) < z < f(x, y) + h(t, x, y)\}\end{aligned}$$

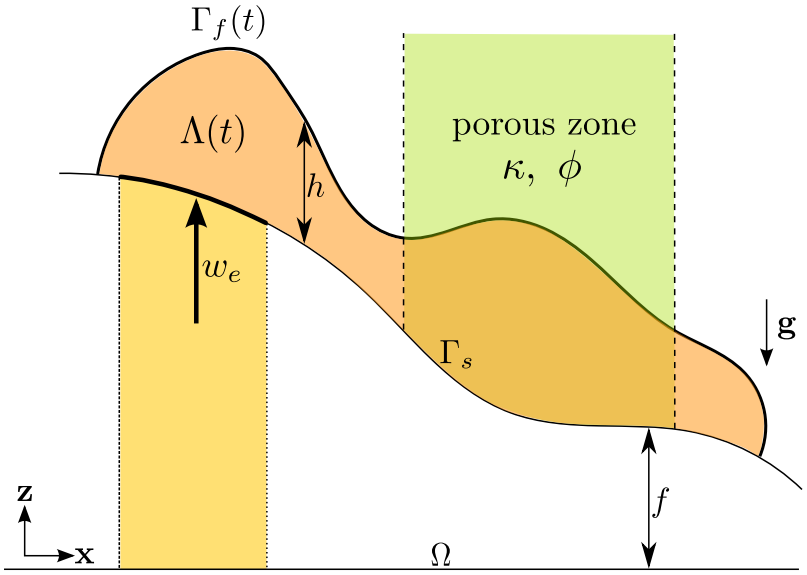

Figure 1: 2D schematic view of a flow on a variable topography, supplied through a vent at the speed w_e, passing through a porous zone with a permeability $\boldsymbol{\kappa}$ and a porosity ϕ.

For any $t > 0$, the boundary conditions at the flow base are a no-slip condition, an imposed vertical speed and natural zero stress on the free surface:

$$u_x = u_y = 0 \text{ and } u_z = w_e \text{ on } \Gamma_s \text{ and } \mathbf{u} = \mathbf{0} \text{ on } \Gamma_w \quad (6)$$

$$\boldsymbol{\sigma} \cdot \boldsymbol{\nu} = 0 \text{ on } \Gamma_f(t) \quad (7)$$

where $\boldsymbol{\nu}$ denotes the unit outward vector of $\partial\Lambda(t)$ on $\Gamma_f(t)$. The imposed vertical speed w_e corresponds to a supply speed of an injection or a lava eruption. Its value is zero beyond the vent.

It remains to describe the evolution of the free surface. It is convenient to introduce the level set function φ that expresses as:

$$\varphi(t, x, y, z) = z - f(x, y) - h(t, x, y).$$

Notice that the zero level set, where $\varphi(t, x, y, z) = 0$, is exactly the free surface. The level set function is transported by the flow: $\partial_t\varphi + \mathbf{u} \cdot \boldsymbol{\nabla}\varphi = 0$,. On $\Gamma_s(t)$, where $z = f + h$, this writes:

$$\partial_t h + u_x\partial_x(f + h) + u_y\partial_y(f + h) - u_z = 0, \ \forall t > 0 \text{ and } (x, y) \in \Omega. \quad (8)$$

This is a first-order transport equation for the height h that should be supplemented by an initial condition:

$$h(t = 0, x, y) = h_{\text{init}}(x, y), \ \forall (x, y) \in \Omega. \quad (9)$$

where h_{init} is given. The set of equation is finally completed by an initial condition for the velocity $\mathbf{u}$:

$$\mathbf{u}(t = 0) = \mathbf{u}_{\text{init}} \text{ in } \Lambda(0) \quad (10)$$

.

To summarize, the three-dimensional problem is composed by the equations (1)-(10) and involves the following unknows: the stress tensor τ, the velocity field $\mathbf{u}$, pressure p, the Darcy source $\mathbf{f}_p$ and the height h.

2.2 Asymptotic shallow analysis

The dimensionless procedure

In this paragraph, we extend the asymptotic analysis developed in [5] for a case of tridimensional flow on a arbitrarilly topography to the case of a flow through a fibrous porous zone. Let H be a characteristic length of the bidimensional domain Ω and H a characteristic height of the flow. We introduce the dimensionless parameter $\varepsilon = H/L$. Let $U = \rho g H^3/(\eta L)$ be a characteristic flow velocity in the (x, y) plane and $g = |\mathbf{g}|$ is the gravity constant. Let $W = \varepsilon U$ be a characteristic velocity in the z direction, $T = L/U$ a characteristic time, and $P = \rho g H$ a characteristic pressure. The problem is reformulated with dimensionless quantities and unknowns, denoted with tildes:

$$
\begin{aligned}
x = L\tilde{x}, y = L\tilde{y}, z = H\tilde{z}, t = T\tilde{t}, p = P\tilde{p}, h = H\tilde{h},\\
u_x = U\tilde{u}_x, u_y = U\tilde{u}_y, u_z = \varepsilon U\tilde{u}_z, w_e = \varepsilon U\tilde{w}_e\\
f_{p,x} = \frac{\eta U}{\kappa_{\|}}\tilde{f}_{p,x},\ f_{p,y} = \frac{\eta U}{\kappa_{\|}}\tilde{f}_{p,y},\ f_{p,z} = \varepsilon\frac{\eta U}{\kappa_{\perp}}\tilde{f}_{p,z}.
\end{aligned}
$$

Remark the non-isotropic scaling procedure for the z coordinate and the z vector component of the velocity vector $\mathbf{u}$. The dimensionless rate of deformation tensor $\tilde{\dot{\boldsymbol{\gamma}}}$ is also related to its dimensional counterpart $\dot{\boldsymbol{\gamma}} = \nabla\mathbf{u} + \nabla\mathbf{u}^T$ by the following non-isotropic relations:

$$
\begin{aligned}
\dot{\gamma}_{\alpha\beta} &= (U/L)\,\tilde{\dot{\gamma}}_{\alpha\beta}, \quad \alpha,\beta \in \{x, y\}\\
\dot{\gamma}_{\alpha z} &= (U/H)\,\tilde{\dot{\gamma}}_{\alpha z}, \quad \alpha \in \{x, y\}\\
\dot{\gamma}_{zz} &= (U/L)\,\tilde{\dot{\gamma}}_{zz}.
\end{aligned}
$$

The scalling procedure for the deviatoric part of stress τ is similar:

$$
\begin{aligned}
\tau_{\alpha\beta} &= \eta\,(U/L)\,\tilde{\tau}_{\alpha\beta}, \quad \alpha,\beta \in \{x, y\},\\
\tau_{\alpha z} &= \eta\,(U/H)\,\tilde{\tau}_{\alpha z}, \quad \alpha \in \{x, y\},\\
\tau_{zz} &= \eta\,(U/L)\,\tilde{\tau}_{zz}.
\end{aligned}
$$

The constitutive equation

The dimensionless rate of deformation tensor can be expressed versus the dimensionless velocity as:

$$
\begin{aligned}
\tilde{\dot{\gamma}}_{\alpha\beta} &= \partial_{\tilde{\beta}}\tilde{u}_\alpha + \partial_{\tilde{\alpha}}\tilde{u}_\beta, \quad \alpha,\beta \in \{x, y\},\\
\tilde{\dot{\gamma}}_{\alpha z} &= \partial_{\tilde{z}}\tilde{u}_\alpha + \varepsilon^2\partial_{\tilde{\alpha}}\tilde{u}_z, \quad \alpha \in \{x, y\},\\
\tilde{\dot{\gamma}}_{zz} &= 2\partial_{\tilde{z}}\tilde{u}_z.
\end{aligned}
$$

The tensor norm scales as: $|\dot{\boldsymbol{\gamma}}| = (U/H)\, E$, where by using (3), we get:

$$\begin{aligned} E &= \big\{\varepsilon^2(\partial_{\tilde{x}}\tilde{u}_y + \partial_{\tilde{y}}\tilde{u}_x)^2 + 2\varepsilon^2(\partial_{\tilde{x}}\tilde{u}_x)^2 + 2\varepsilon^2(\partial_{\tilde{y}}\tilde{u}_y)^2 \\ &\quad +2\varepsilon^2(\partial_{\tilde{x}}\tilde{u}_x + \partial_{\tilde{y}}\tilde{u}_y)^2 + (\partial_{\tilde{z}}\tilde{u}_x + \varepsilon^2\partial_{\tilde{x}}\tilde{u}_z)^2 + (\partial_{\tilde{z}}\tilde{u}_y + \varepsilon^2\partial_{\tilde{y}}\tilde{u}_z)^2\big\}^{\frac{1}{2}} \end{aligned}$$

Let us introduce the Bingham dimensionless number Bi that compares the yield stress τ_y to a characteristic viscous stress $\eta U/H$:

$$Bi = \frac{\tau_y H}{\eta U} = \varepsilon^{-1}\frac{\tau_y}{\rho g H}.$$

We suppose that $Bi = \mathcal{O}(1)$ in ε. This hypothesis interprets as $\tau_y/(\rho g H) = \mathcal{O}(\varepsilon)$ or equivalently that the yield stress τ_y is supposed to be small when compared to the gravity effets $\rho g H$. When $|\boldsymbol{\tau}| \geqslant \tau_y$ we obtain a dimensionless version of the constitutive equation (1):

$$\tilde{\tau}_{ij} = \left(\frac{Bi}{E} + 1\right)\tilde{\dot{\gamma}}_{ij}$$

Then $|\boldsymbol{\tau}| = \eta(U/H)T$ where:

$$T = \left\{\tilde{\tau}_{xz}^2 + \tilde{\tau}_{yz}^2 + \frac{1}{2}\varepsilon^2\tilde{\tau}_{xx}^2 + \frac{1}{2}\varepsilon^2\tilde{\tau}_{yy}^2 + \frac{1}{2}\varepsilon^2\tilde{\tau}_{zz}^2 + \varepsilon^2\tilde{\tau}_{xy}^2\right\}^{\frac{1}{2}}.$$

Remark that the von Mises condition $|\boldsymbol{\tau}| \geqslant \tau_y$ then becomes $T \geqslant Bi$. The constitutive equation (1) writes:

$$\begin{cases} \tilde{\boldsymbol{\tau}} = \left[\frac{Bi}{E} + 1\right]\tilde{\dot{\boldsymbol{\gamma}}} & \text{when } E \neq 0, \\ T \leqslant Bi & \text{otherwise.} \end{cases} \tag{11}$$

The Darcy source term equation

The anisotropic norm of velocity scales as: $|\boldsymbol{A}\mathbf{u}| = |\boldsymbol{A}|UV$ where:

$$V = \frac{\left(A_{xx}^2\tilde{u}_x^2 + A_{yy}^2\tilde{u}_y^2 + \varepsilon^2 A_{zz}^2\tilde{u}_z^2\right)^{1/2}}{|\boldsymbol{A}|}.$$

Let us introduce the Darcy-Bingham dimensionless number Bi_p that compares the yield stress τ_y to a characteristic viscous stress in fibrous porous medium $\eta U|\boldsymbol{A}|$:

$$Bi_p = \frac{\tau_y}{\eta U|\boldsymbol{A}|} = \frac{1}{H|\boldsymbol{A}|}Bi.$$

We suppose that $Bi_p = \mathcal{O}(1)$ in ε. This hypothesis interprets as $\tau_y|\boldsymbol{A}|/(\rho g) = \mathcal{O}(\varepsilon)$ or equivalently that the yield stress τ_y is supposed to be small when compared to the gravity effets in a porous medium $\rho g/|\boldsymbol{A}|$. When $\mathbf{u} \neq \mathbf{0}$ we obtain a dimensionless version of the Darcy source term equation (5):

$$\tilde{\mathbf{f}}_p = -\left(\frac{Bi_p}{V} + 1\right)\tilde{\mathbf{u}}$$

The Darcy source term norm scales as: $|\boldsymbol{A\kappa f}_p| = |A|\eta UF$ where

$$F = \frac{\left(A_{xx}^2 \tilde{f}_{p,x}^2 + A_{yy}^2 \tilde{f}_{p,y}^2 + \varepsilon^2 A_{zz}^2 \tilde{f}_{p,z}^2\right)^{1/2}}{|\boldsymbol{A}|}.$$

Then, the threshold condition $|\boldsymbol{A\kappa f}_p| \leqslant \tau_y$ becomes $F < Bi_p$ and the Darcy source term equation (5) writes:

$$\begin{cases} \tilde{\mathbf{f}}_p = -\left(\dfrac{Bi_p}{V} + 1\right)\tilde{\mathbf{u}}, & \text{when } \tilde{\mathbf{u}} \neq \mathbf{0}, \\ F < Bi_p & \text{when } \tilde{\mathbf{u}} = \mathbf{0}, \end{cases} \tag{12}$$

The conservation equations

Let us introduce the Reynolds number and Darcy numbers:

$$Re = \frac{\rho UL}{\eta} = \frac{\rho^2 g H^3}{\eta^2}, \qquad Da_{\parallel} = \frac{\kappa_{\parallel}}{H^2}, \qquad Da_{\perp} = \frac{\kappa_{\perp}}{H^2}.$$

We suppose that $Re = \mathcal{O}(1)$ in ε which means that the flow is supposed to be sufficiently slow for the inertia effects to be neglected at the zeroth order of development in ε. We suppose also that $Da_{\parallel} = \mathcal{O}(1)$ and $Da_{\perp} = \mathcal{O}(1)$ which means that the presence of a porous medium has an influence on the horizontal flow but nothing for the vertical flow.

The conservation of momentum and mass (2)-(3) become:

$$\varepsilon^2 Re(\partial_{\tilde{t}}\tilde{u}_x + \tilde{u}_x\partial_{\tilde{x}}\tilde{u}_x + \tilde{u}_y\partial_{\tilde{y}}\tilde{u}_x + \tilde{u}_z\partial_{\tilde{z}}\tilde{u}_x) = -\partial_{\tilde{x}}\tilde{p} + \varepsilon^2(\partial_{\tilde{x}}\tilde{\tau}_{xx} + \partial_{\tilde{y}}\tilde{\tau}_{xy}) \tag{13a}$$

$$+ \partial_{\tilde{z}}\tilde{\tau}_{xz} + Da_{\parallel}^{-1}\tilde{f}_{p,x}, \tag{13b}$$

$$\varepsilon^2 Re(\partial_{\tilde{t}}\tilde{u}_y + \tilde{u}_x\partial_{\tilde{x}}\tilde{u}_y + \tilde{u}_y\partial_{\tilde{y}}\tilde{u}_y + \tilde{u}_z\partial_{\tilde{z}}\tilde{u}_y) = -\partial_{\tilde{y}}\tilde{p} + \varepsilon^2(\partial_{\tilde{x}}\tilde{\tau}_{xy} + \partial_{\tilde{y}}\tilde{\tau}_{yy}) \tag{13c}$$

$$+ \partial_{\tilde{z}}\tilde{\tau}_{yz} + Da_{\parallel}^{-1}\tilde{f}_{p,y}, \tag{13d}$$

$$\varepsilon^4 Re(\partial_{\tilde{t}}\tilde{u}_z + \tilde{u}_x\partial_{\tilde{x}}\tilde{u}_z + \tilde{u}_y\partial_{\tilde{y}}\tilde{u}_z + \tilde{u}_z\partial_{\tilde{z}}\tilde{u}_z) = -\partial_{\tilde{z}}\tilde{p} + \varepsilon^2(\partial_{\tilde{x}}\tilde{\tau}_{xz} + \partial_{\tilde{y}}\tilde{\tau}_{yz} + \partial_{\tilde{z}}\tilde{\tau}_{zz}) \tag{13e}$$

$$- 1 + \varepsilon Da_{\perp}^{-1}\tilde{f}_{p,z}, \tag{13f}$$

$$\partial_{\tilde{x}}\tilde{u}_x + \partial_{\tilde{y}}\tilde{u}_y + \partial_{\tilde{z}}\tilde{u}_z = 0. \tag{13g}$$

Boundary and initial conditions

The no-slip boundary condition (6) writes:

$$\tilde{u}_x = \tilde{u}_y = 0 \text{ and } \tilde{u}_z = \tilde{w}_e \text{ on } \Gamma_s \text{ and } \tilde{\mathbf{u}} = \mathbf{0} \text{ on } \Gamma_w$$

The unit outward normal $\boldsymbol{\nu}$ on the free surface $\Gamma_s(t)$ expresses as:

$$\boldsymbol{\nu} = \frac{\boldsymbol{\nabla}\varphi}{||\boldsymbol{\nabla}\varphi||} = \frac{1}{\sqrt{1 + |\boldsymbol{\nabla}(f+h)|^2}} \begin{pmatrix} -\partial_x(f+h) \\ -\partial_y(f+h) \\ 1 \end{pmatrix}.$$

Then (7) writes:

$$\begin{pmatrix} \tau_{xx}-p & \tau_{xy} & \tau_{xz} \\ \tau_{xy} & \tau_{yy}-p & \tau_{yz} \\ \tau_{xz} & \tau_{yz} & \tau_{zz}-p \end{pmatrix} \begin{pmatrix} -\partial_x(f+h) \\ -\partial_y(f+h) \\ 1 \end{pmatrix} = \begin{pmatrix} 0 \\ 0 \\ 0 \end{pmatrix}.$$

and becomes in dimensionless form:

$$\begin{aligned} -(\varepsilon^2\tilde{\tau}_{xx}-\tilde{p})\partial_{\tilde{x}}(\tilde{f}+\tilde{h}) - \varepsilon^2\tilde{\tau}_{xy}\partial_{\tilde{y}}(\tilde{f}+\tilde{h}) + \tilde{\tau}_{xz} &= 0 \quad (14a) \\ -\varepsilon^2\tilde{\tau}_{xy}\partial_{\tilde{x}}(\tilde{f}+\tilde{h}) - (\varepsilon^2\tilde{\tau}_{yy}-\tilde{p})\partial_{\tilde{y}}(\tilde{f}+\tilde{h}) + \tilde{\tau}_{yz} &= 0 \quad (14b) \\ -\varepsilon^2\tilde{\tau}_{xz}\partial_{\tilde{x}}(\tilde{f}+\tilde{h}) - \varepsilon^2\tilde{\tau}_{yz}\partial_{\tilde{y}}(\tilde{f}+\tilde{h}) + \varepsilon^2\tilde{\tau}_{zz} - \tilde{p} &= 0 \quad (14c) \end{aligned}$$

where $\tilde{f} = f/H$ denotes the dimensionless topography and is known. The transport equation (8) for the flow height h becomes:

$$\partial_{\tilde{t}}\tilde{h} + \tilde{u}_x\partial_{\tilde{x}}(\tilde{f}+\tilde{h}) + \tilde{u}_y\partial_{\tilde{y}}(\tilde{f}+\tilde{h}) - \tilde{u}_z = 0. \quad (15)$$

The dimensionless problem is completed by the initial conditions for the dimensionless height and velocity. The initial (1)-(10) problem and its dimensionless version are equivalent, since the change of unknowns is simply linear.

2.3 The zeroth order approximation

In this paragraph, we only consider the dimensionless problem: since there is no ambiguity, we omit the tilde on the dimensionless variables. We assume that the unknowns admit the following development in ε when $\varepsilon \ll 1$:

$$\begin{aligned} \boldsymbol{\tau} &= \boldsymbol{\tau}_0 + \varepsilon\boldsymbol{\tau}_1 + \varepsilon^2\boldsymbol{\tau}_2 + \dots \\ \mathbf{u} &= \mathbf{u}_0 + \varepsilon\mathbf{u}_1 + \varepsilon^2\mathbf{u}_2 + \dots \\ p &= p_0 + \varepsilon p_1 + \varepsilon^2 p_2 + \dots \\ h &= h_0 + \varepsilon h_1 + \varepsilon^2 h_2 + \dots \\ \mathbf{f}_p &= \mathbf{f}_{p,0} + \varepsilon\mathbf{f}_{p,1} + \varepsilon^2\mathbf{f}_{p,2} + \dots \end{aligned}$$

In this paragraph, we aim at obtaining the problem at the zero order for $\boldsymbol{\tau}_0$, $\mathbf{u}$, p_0 and h_0. Since we only consider the zeroth order, we also omit the zero subscript in this paragraph. Let us denote $\boldsymbol{\nabla}_\parallel = (\partial_x, \partial_y)$ the gradient vector in the Oxy plane, $\mathbf{u}_\parallel = (u_x, u_y)$ and $\mathbf{f}_{p,\parallel} = (f_{p,x}, f_{p,y})$, the projected velocity and Darcy's force in this plane and $\boldsymbol{\tau}_\parallel = (\tau_{xz}, \tau_{yz})$ the shear stress vector in the same plane. For any $\mathbf{v}_\parallel = (v_x, v_y)$ we also denote as $\mathrm{div}_\parallel \mathbf{v}_\parallel = \partial_x v_x + \partial_y v_y$ the corresponding plane divergence and $\left|\mathbf{v}_\parallel\right| = (v_x^2 + v_y^2)^{1/2}$ the usual Euclidean norm in $\mathbb{R}^2$. For convenience, we also denote as $\mathbf{dir}\left(\mathbf{v}_\parallel\right) = \mathbf{v}_\parallel / \left|\mathbf{v}_\parallel\right|$ the direction of any nonzero plane vector. With these notations, we have $E = \left|\partial_z \mathbf{u}_\parallel\right|$, $T = \left|\boldsymbol{\tau}_\parallel\right|$ and $V = \dfrac{A_\parallel}{|\boldsymbol{A}|}\left|\mathbf{u}_\parallel\right|$, $F = \dfrac{A_\parallel}{|\boldsymbol{A}|}\left|\mathbf{f}_{p,\parallel}\right|$ at the zeroth order, where $A_\parallel := A_{xx} = A_{yy} = \dfrac{\alpha_\parallel}{\sqrt{\kappa_\parallel \phi}}$.

The constitutive equation (11) then reduces to:

$$\tau_{\alpha z} = \left[\frac{Bi}{\left|\partial_z \mathbf{u}_\parallel\right|} + 1\right] \partial_z u_\alpha, \quad \forall \alpha \in \{x, y\}, \tag{16a}$$

$$\tau_{\alpha\beta} = \left[\frac{Bi}{\left|\partial_z \mathbf{u}_\parallel\right|} + 1\right] (\partial_\beta u_\alpha + \partial_\alpha u_\beta), \quad \forall \alpha, \beta \in \{x, y\}, \tag{16b}$$

$$\tau_{zz} = 2\left[\frac{Bi}{\left|\partial_z \mathbf{u}_\parallel\right|} + 1\right] \partial_z u_z, \tag{16c}$$

when $\partial_z \mathbf{u}_\parallel \neq \mathbf{0}$ and

$$\left|\boldsymbol{\tau}_\parallel\right| \leqslant Bi, \quad \text{otherwise.} \tag{16d}$$

The Darcy's force equation (12) then reduces to:

$$\begin{cases} \mathbf{f}_p = -\left(\dfrac{Bi_{p,\parallel}}{\left|\mathbf{u}_\parallel\right|} + 1\right) \mathbf{u}, & \text{when } \mathbf{u}_\parallel \neq \mathbf{0}, \\ \left|\mathbf{f}_{p,\parallel}\right| \leqslant Bi_{p,\parallel} & \text{when } \mathbf{u}_\parallel = \mathbf{0}, \end{cases} \tag{17}$$

where $Bi_{p,\parallel} = \dfrac{|\boldsymbol{A}|}{A_\parallel} Bi_p = \dfrac{\sqrt{\kappa_\parallel \phi}}{H \alpha_\parallel} Bi$.

From the conservation laws (13) we get at the zeroth order:

$$\partial_z \tau_{xz} - \partial_x p + Da_\parallel^{-1} f_{p,x} = 0, \tag{18a}$$

$$\partial_z \tau_{yz} - \partial_y p + Da_\parallel^{-1} f_{p,y} = 0, \tag{18b}$$

$$-\partial_z p = -1, \tag{18c}$$

$$\partial_x u_x + \partial_y u_y + \partial_z u_z = 0. \tag{18d}$$

The free surface boundary condition (14) at $z = f(x, y) + h(t, x, y)$ reduces at the zeroth order to:

$$\tau_{xz} + p\partial_x(f + h) = 0, \tag{19a}$$

$$\tau_{yz} + p\partial_y(f + h) = 0, \tag{19b}$$

$$p = 0. \tag{19c}$$

The velocity condition at the base ($z = f(x, y)$) remains unchanged but using the projected velocity, its writes:

$$\mathbf{u}_\parallel = \mathbf{0}, \tag{20a}$$

$$u_z = w_e. \tag{20b}$$

The others equations, i.e. the transport equation (15), the no-slip boundary condition on walls and the initial conditions for $\mathbf{u}$ and h remains unchanged at the zeroth order.

2.4 Reducing the problem

In this paragraph, we show that the zeroth order problem reduces to a nonlinear parabolic problem involving only one unknow h. All the others quantities $\boldsymbol{\tau}$, $\mathbf{u}$, p and $\mathbf{f}_p$ at the zeroth order can be explicitly computed from h.

From (19) we get at the free surface $z = f + h$:

$$p(z=f+h) = 0, \tag{21a}$$
$$\boldsymbol{\tau}_{\|}(z=f+h) = \mathbf{0}. \tag{21b}$$

Integrating (18c) in z from $z = 0$ to $z = f + h$ and using (21a), we have:

$$p(t,x,y,z) = f(x,y) + h(t,x,y) - z. \tag{22}$$

As f is known, the quantity p depends only upon the unknown h. From the conservation laws (18a)-(18b) and the pressure expression (22), we get:

$$\partial_z \boldsymbol{\tau}_{\|} + Da_{\|}^{-1}\mathbf{f}_{p,\|} = \boldsymbol{\nabla}_{\|}(f+h). \tag{23}$$

To find more easily an expression of $\mathbf{u}_{\|}$ involving the only unknow h from the set of equations, we can make some assumptions on the velocity profile $\mathbf{u}_{\|}$ and shear stress vector $\boldsymbol{\tau}$ based on the profiles obtained in the previous paper [5] given by the equations (21) and (18). We assume that the solutions has the same form: $\mathbf{u}_{\|} = -g(z)\boldsymbol{\nabla}_{\|}(f+h)$ where the function g is in $\mathcal{C}^1([f,f+h],\mathbb{R}^+) \cap \mathcal{D}^2([f,f+h],\mathbb{R}^+)$, and $\boldsymbol{\tau}_{\|} = -\tau(z)\boldsymbol{\nabla}_{\|}(f+h)$ where the function τ is in $\mathcal{C}^1([f,f+h],\mathbb{R}^+)$. Let us first deal with the particular case where $\boldsymbol{\nabla}_{\|}(f+h) = \mathbf{0}$. In this case, $\mathbf{u}_{\|} = \mathbf{0}$, $\boldsymbol{\tau}_{\|} = \mathbf{0}$ and by (23), $\mathbf{f}_{p,\|} = \mathbf{0}$. Otherwise, when $\boldsymbol{\nabla}_{\|}(f+h) \neq \mathbf{0}$, we assume that exits critical height h_c in $[0,h]$ for which the function g is strictly increasing on $[f, f+h_c]$, constant on $]f+h_c, f+h]$ and for which the function τ strictly decreases on $[f, f+h_c]$ and satisfies:

$$\tau(f+h_c) = \frac{Bi}{\left|\boldsymbol{\nabla}_{\|}(f+h)\right|}. \tag{24}$$

Remark that for all points $(x,y) \in \Omega$, as g is stricly increasing on $[f, f+h]$, constant on $]f+h_c, f+h]$ and $\mathbf{u}_{\|}(z=f) = \mathbf{0}$, thus an equivalent condition of $\mathbf{u}_{\|} = \mathbf{0}, \forall z \in [f, f+h]$ is $h_c = 0$. From the equation (16a), the von Mises condition (16d) and assumptions on g, we get:

$$\begin{cases} \boldsymbol{\tau}_{\|} = -\left(\frac{Bi}{\left|\boldsymbol{\nabla}_{\|}(f+h)\right|} + g'(z)\right)\boldsymbol{\nabla}_{\|}(f+h), & \text{when } z \in [f, f+h_c], \\ \left|\boldsymbol{\tau}_{\|}\right| \leqslant Bi, & \text{when } z \in]f+h_c, f+h]. \end{cases} \tag{25}$$

From the Darcy's force equation (17) projected on the plane Oxy and assumptions on g, we get:

$$\begin{cases} \mathbf{f}_{p,\|}(z) = \left(\frac{Bi_{p,\|}}{\left|\boldsymbol{\nabla}_{\|}(f+h)\right|} + g(z)\right)\boldsymbol{\nabla}_{\|}(f+h), & \text{when } h_c > 0, \\ \left|\mathbf{f}_{p,\|}\right| \leqslant Bi_{p,\|} & \text{when } h_c = 0. \end{cases} \tag{26}$$

Let us describe the equation (23) is the case where $h_c > 0$. By using the expression of $\boldsymbol{\tau}_\parallel$ (25) and the expression of $\mathbf{f}_{p,\parallel}$ (26), it gives the following scalar equations

$$g''(z) - Da_\parallel^{-1} g(z) = \frac{Da_\parallel^{-1} Bi_{p,\parallel}}{\left|\boldsymbol{\nabla}_\parallel (f+h)\right|} - 1, \text{ when } z \in [f, f+h_c], \tag{27}$$

$$\tau'(z) = Da_\parallel^{-1} \left(g(f+h_c) + \frac{Bi_{p,\parallel}}{\left|\boldsymbol{\nabla}_\parallel (f+h)\right|} \right) - 1, \text{ when } z \in]f+h_c, f+h]. \tag{28}$$

Equation (27) is a second-order linear ODE with z-independent coefficients, with a discriminant $\Delta = 4Da_\parallel^{-1}$. Thus, it exists α and β independents of z such that:

$$g(z) = \alpha \exp\left(Da_\parallel^{-1/2} z\right) + \beta \exp\left(-Da_\parallel^{-1/2} z\right) + Da_\parallel \left(1 - \frac{Da_\parallel^{-1} Bi_{p,\parallel}}{\left|\boldsymbol{\nabla}_\parallel (f+h)\right|}\right), \text{ for } z \in [f, f+h_c] \tag{29}$$

Here, α, β are determined by the boundary conditions. The no-slip condition on the basal topography write:

$$g(f) = 0.$$

The assumption on g to be constant on $]f+h_c, f+h]$ and $\mathcal{C}^1$ on $[f, f+h]$ leads to the second condition when $h_c < h$:

$$g'(f+h_c) = 0. \tag{30}$$

Remark that when $h_c = h$, the condition (30) stays valid. Indeed, from the value of τ in $z = f + h_c = f + h$ given by (24) and the boundary condition (21b), we get $Bi = 0$. Thus by using the expression of $\boldsymbol{\tau}_\parallel$ in $z = f + h_c = f + h$ given in (25), it comes again the equation (30).

Writing these boundary conditions with the expression of g (29) leads to:

$$\alpha \exp\left(Da_\parallel^{-1/2} f\right) + \beta \exp\left(-Da_\parallel^{-1/2} f\right) = Da_\parallel \left(\frac{Da_\parallel^{-1} Bi_{p,\parallel}}{\left|\boldsymbol{\nabla}_\parallel (f+h)\right|} - 1 \right), \tag{31}$$

$$\alpha \exp\left(Da_\parallel^{-1/2} (f+h_c)\right) - \beta \exp\left(-Da_\parallel^{-1/2} (f+h_c)\right) = 0, \tag{32}$$

This linear system in terms of α and β solves as:

$$\begin{cases} \alpha = Da_\parallel \left(\dfrac{Da_\parallel^{-1} Bi_{p,\parallel}}{\left|\boldsymbol{\nabla}_\parallel (f+h)\right|} - 1 \right) \dfrac{\exp\left(-Da_\parallel^{-1/2} (f+h_c)\right)}{2\cosh\left(Da_\parallel^{-1/2} h_c\right)} & (33) \\ \beta = Da_\parallel \left(\dfrac{Da_\parallel^{-1} Bi_{p,\parallel}}{\left|\boldsymbol{\nabla}_\parallel (f+h)\right|} - 1 \right) \dfrac{\exp\left(Da_\parallel^{-1/2} (f+h_c)\right)}{2\cosh\left(Da_\parallel^{-1/2} h_c\right)} & (34) \end{cases}$$

It remains to characterize from the input data an equivalent condition of $h_c < h$ and a relation to determine h_c. We have already seen that $h_c = h$ implies $Bi = 0$. It can

be proved that the reverse is true. Indeed, suppose that $Bi = 0$. From (24) and (21b), $\boldsymbol{\tau}_{\|}(f + h_c) = \boldsymbol{\tau}_{\|}(f + h) = \mathbf{0}$. Integrate between $f + h_c$ and $f + h$ the equation (23) and using the expression of Darcy's force given in (26), it gives:

$$\int_{f+h_c}^{f+h} g(z)\mathrm{d}z = Da_{\|}(h - h_c) \tag{35}$$

The function g is constant on the interval $[f + h_c, f + h]$. Thus, from the expression of g (29), forall $z \in [f + h_c, f + h]$,

$$g(z) = g(f + h_c) = Da_{\|} - \frac{Da_{\|}}{\cosh\left(Da_{\|}^{-1/2} h_c\right)}.$$

Finally, from the egality (35), it comes $h_c = h$, proving the equivalence: $h_c = h \Leftrightarrow Bi = 0$. It remains to determine h_c from the input data when $Bi \neq 0 \Leftrightarrow h_c \in [0, h[$. By integrating the equation (28) between $f + h_c$ and $f + h$ and using (21b), we get:

$$(h - h_c)\ g(f + h_c) = \left(Da_{\|} - \frac{Bi_{p,\|}}{\left|\boldsymbol{\nabla}_{\|}(f + h)\right|}\right)(h - h_c) - \frac{Da_{\|} Bi}{\left|\boldsymbol{\nabla}_{\|}(f + h)\right|}. \tag{36}$$

Writing this equation with the expression of g (29) gives:

$$(h - h_c)\left(\alpha \exp\left(Da_{\|}^{-1/2}(f + h_c)\right) + \beta \exp\left(-Da_{\|}^{-1/2}(f + h_c)\right)\right) = -\frac{Da_{\|} Bi}{\left|\boldsymbol{\nabla}_{\|}(f + h)\right|}.$$

At last, using the expressions of α and β from (33) and (34) in the previous equation, we get a relation on h_c:

$$Bi\ \cosh\left(Da_{\|}^{-1/2} h_c\right) = (h - h_c)\left(\left|\boldsymbol{\nabla}_{\|}(f + h)\right| - Da_{\|}^{-1} Bi_{p,\|}\right) \tag{37}$$

This expression gives a necessary condition so that $h_c > 0$. Firstly, as $Bi\ \cosh\left(Da_{\|}^{-1/2} h_c\right)$ and $(h - h_c)$ are strictly positives when $0 < h_c < h$, necessarly, $\left|\boldsymbol{\nabla}_{\|}(f + h)\right| - Da_{\|}^{-1} Bi_{p,\|} > 0$. The inequation still true when $h_c = h$ because in this case $Bi_{p,\|} = 0$. We deduce a more general necessary condition:

$$\begin{aligned} h_c > 0 &\Rightarrow h_c\left(\left|\boldsymbol{\nabla}_{\|}(f + h)\right| - Da_{\|}^{-1} Bi_{p,\|}\right) > 0 \\ &\Rightarrow h\left(\left|\boldsymbol{\nabla}_{\|}(f + h)\right| - Da_{\|}^{-1} Bi_{p,\|}\right) > Bi \cosh\left(Da_{\|}^{-1/2} h_c\right) \\ &\Rightarrow h\left(\left|\boldsymbol{\nabla}_{\|}(f + h)\right| - Da_{\|}^{-1} Bi_{p,\|}\right) > Bi \end{aligned}$$

The reverse is also true which gives a necessary and sufficient condition for $h_c > 0$. Let us prove it by contrapositive. If $h_c = 0$, integrating between $f + h_c$ and $f + h$ the equation (23):

$$\boldsymbol{\nabla}_{\|}(f+h)\left(h-\frac{Bi}{\left|\boldsymbol{\nabla}_{\|}(f+h)\right|}\right)=Da_{\|}^{-1}\int_{f}^{f+h}\mathbf{f}_{\|}\mathrm{d}z$$

Take the norm and use the threshold condition from (26) that gives:

$$\left|h\left|\boldsymbol{\nabla}_{\|}(f+h)\right|-Bi\right|=Da_{\|}^{-1}\left|\int_{f}^{f+h}\mathbf{f}_{\|}\mathrm{d}z\right|\leqslant Da_{\|}^{-1}\int_{f}^{f+h}\left|\mathbf{f}_{\|}\right|\mathrm{d}z\leqslant Da_{\|}^{-1}Bi_{p,\|}\;h \tag{38}$$

By definition, $h\left|\boldsymbol{\nabla}_{\|}(f+h)\right|-Bi\leqslant\left|h\left|\boldsymbol{\nabla}_{\|}(f+h)\right|-Bi\right|$ which gives with the inegality (38):

$$h\left(\left|\boldsymbol{\nabla}_{\|}(f+h)\right|-Da_{\|}^{-1}Bi_{p,\|}\right)\leqslant Bi.$$

Define for all $z\in]0,h]$ and $h,\ \xi$ in $\mathbb{R}^{+}$ the function:

$$F_{h,\xi}(z)=Bi\cosh\left(Da_{\|}^{-1/2}z\right)+(z-h)\left(\xi-Da_{\|}^{-1}Bi_{p,\|}\right)$$

Note that the function $z\longmapsto F_{h,\xi}(z)$ is an invertible function in $]0,h]$ when $\left(\xi-Da_{\|}^{-1}Bi_{p,\|}\right)>0$. Use the equivalent $h_c>0\Leftrightarrow h\left(\left|\boldsymbol{\nabla}_{\|}(f+h)\right|-Da_{\|}^{-1}Bi_{p,\|}\right)>Bi$ leads to a general expression for $h_c=h_c(h,\left|\boldsymbol{\nabla}_{\|}(f+h)\right|)$ where

$$h_c(h,\xi)=\begin{cases}0 & \text{when } h\left(\xi-Da_{\|}^{-1}Bi_{p,\|}\right)\leqslant Bi,\\ F_{h,\xi}^{-1}(0) & \text{when } h\left(\xi-Da_{\|}^{-1}Bi_{p,\|}\right)>Bi.\end{cases} \tag{39}$$

In pratice, the value of h_c for a given h and ξ is efficiently computed by a Newton algorithm and the machine precision is reached in few iterations.

Finally, the general expression of g writes:

$$g(z)=\begin{cases}\left(\dfrac{Bi_{p,\|}}{\left|\boldsymbol{\nabla}_{\|}(f+h)\right|}-Da_{\|}\right)\left(\dfrac{\cosh\left(Da_{\|}^{-1/2}(f+h_c-z)\right)}{\cosh\left(Da_{\|}^{-1/2}h_c\right)}-1\right) & \text{when } z\in[f,f+h_c],\\ \left(\dfrac{Bi_{p,\|}}{\left|\boldsymbol{\nabla}_{\|}(f+h)\right|}-Da_{\|}\right)\left(\dfrac{1-\cosh\left(Da_{\|}^{-1/2}h_c\right)}{\cosh\left(Da_{\|}^{-1/2}h_c\right)}\right) & \text{when } z\in\,]f+h_c,f+h].\end{cases} \tag{40}$$

The last component of the velocity is obtained by integrating the mass conservation (13g) in $[f,z]$:

$$\int_{f}^{z}\partial_x u_x\mathrm{d}z+\int_{f}^{z}\partial_y u_y\mathrm{d}z+\int_{f}^{z}\partial_z u_z\mathrm{d}z=0 \tag{41}$$

The condition $u_z = w_e$ in $z = f$ gives:

$$u_z(t,x,y,z) = w_e - \int_{f(x,y)}^{z} \mathrm{div}_{\|}\left(\mathbf{u}_{\|}\right)\, \mathrm{d}z \tag{42}$$

Thus, velocity $\mathbf{u}$ admits an explicit expression depending only upon h. Then, the complete stress $\boldsymbol{\tau}$ follows explicitly from (16). It remains to obtain a characterization of h alone. Let us consider (42) at $z = f + h$: by swapping the derivation ∂_x and ∂_y with the integral over $[f(x,y), f(x,y) + h(t,x,y)]$, and using the no-slip boundary condition at $z = f$, we get:

$$\int_f^{f+h} \partial_\alpha u_\alpha \mathrm{d}z = \partial_\alpha \left(\int_f^{f+h} u_\alpha \mathrm{d}z \right) - u_\alpha(t,x,y,f+h)\partial_\alpha(f+h),\ \forall \alpha \in \{x,y\}$$

Combining the previous relation with the transport equation (15) at the zeroth order, and replacing in (42) at $z = f + h$, leads to:

$$\partial_t h + \mathrm{div}_{\|} \left(\int_f^{f+h} \mathbf{u}_{\|} \mathrm{d}z \right) = w_e$$

By replacing in the previous equation $\mathbf{u}_{\|} = -g\boldsymbol{\nabla}_{\|}(f+h)$ by its expression where g is given in (40), depending only upon h, we obtain, after rearrangements, the following conservative equation for h:

$$\partial_t h - \mathrm{div}_{\|} \left\{ \tilde{\mu}(h,\, |\boldsymbol{\nabla}_{\|}(f+h)|)\ \boldsymbol{\nabla}_{\|}(f+h) \right\} = w_e \ \text{ in }]0,+\infty[\times\Omega \tag{43}$$

Here, $\tilde{\mu}$ denotes a diffusion coefficient, defined for all $h, \xi \in \mathbb{R}^+$ by:

$$\tilde{\mu}(h,\,\xi) = \begin{cases} \left(Da_{\|} - \dfrac{Bi_{p,\|}}{\xi}\right) \left[\left(h - \dfrac{Bi}{\xi - Da_{\|}^{-1} Bi_{p,\|}} \right) - Da_{\|}^{1/2} \tanh\left(Da_{\|}^{-1/2} h_c(h,\xi) \right) \right] & \\ \qquad\qquad \text{when } h_c(h,\xi) > 0, & \\ 0 \qquad\qquad \text{otherwise.} & \end{cases} \tag{44}$$

This expression contains three parameters: Bi from the dimensionless Bingham model and $Bi_{p,\|}$ and $Da_{\|}$ from the dimensionless Darcy source term added in the momentum equation. The no-slip velocity condition at the lateral boundaries leads to an homogeneous Neumann boundary condition:

$$\frac{\partial(f+h)}{\partial n} = 0 \text{ on }]0,+\infty[\times\partial\Omega \tag{45}$$

where $\partial/\partial n = \mathbf{n}.\boldsymbol{\nabla}_{\|}$ and $\mathbf{n}$ denotes the outward unit normal on $\partial\Omega$ in the Oxy plane. Recall the initial condition:

$$h(t{=}0) = h_{\text{init}} \text{ in } \Omega \tag{46}$$

The reduced problem writes: find $h(t,x,y)$, defined for all $t > 0$ and $(x,y) \in \Omega$ and satisfying (43), (45) and (46).

Notice that, for a Newtonian flow ($Bi = 0$), expression (44) simplifies as:

$$\tilde{\mu}(h,\,\xi) = Da_{\|} \left[h - Da_{\|}^{1/2} \tanh\left(Da_{\|}^{-1/2} h \right) \right].$$

Remark that the present model with porous zone is consistent with the model without porous zone developed in [5] (i.e. when $Da_{\|}^{-1} = 0$ and $Bi_{p,\|} = 0$). Indeed, the expression of μ is then obtained by assuming that $Bi_{p,\|} = 0$ and by using a truncated expansion in $r = Da_{\|}^{-1/2}$. Note $h_c = h_{c,0} + rh_{c,1} + r^2h_{c,2} + r^3h_{c,3} + r^4h_{c,4} + o(r^4)$. The relation (37) leads to the following limited development of h_c :

$$h_c = h_{c,0} - \frac{Bih_{c,0}^2}{2\left|\boldsymbol{\nabla}_{\|}(f+h)\right|}r^2 + \frac{Bih_{c,0}^3}{24\left|\boldsymbol{\nabla}_{\|}(f+h)\right|}\left(\frac{13Bi}{\left|\boldsymbol{\nabla}_{\|}(f+h)\right|} - h\right)r^4 + o(r^4)$$

where $h_{c,0} = h - \dfrac{Bi}{\left|\boldsymbol{\nabla}_{\|}(f+h)\right|}$. The expansion at order 4 is necessary to obtain that of $\tilde{\mu}$ at order 2, which is:

$$\tilde{\mu}(h,\xi) = \begin{cases} \dfrac{(2h\xi + Bi)\ (h\xi - Bi)^2}{6\ \xi^3} + r^2\dfrac{Bi(h\xi - Bi)^3(h\xi - 13Bi)}{2\xi^5} + o(r^2) & \text{when } h_c > 0, \\ 0 & \text{otherwise.} \end{cases}$$

By taking the limit when r tends to zero, we find back the formula (25) given in [5] for the Bingham case ($n = 1$).

2.5 The final reduced problem

Going back to dimensional variable, the zeroth order equation (43) for the height h writes:

$$\partial_t h - \left(\frac{\rho g}{\eta}\right)\mathrm{div}_{\|}\left\{\mu\left(h,\ \left|\boldsymbol{\nabla}_{\|}(f+h)\right|\right)\ \boldsymbol{\nabla}_{\|}(f+h)\right\} = w_e \ \text{ in }]0,+\infty[\times\Omega, \tag{47}$$

where μ denotes a diffusion coefficient, defined for all $h, \xi \in \mathbb{R}^+$ by:

$$\mu(h,\ \xi) = \begin{cases} \left(\kappa_{\|} - \dfrac{\tau_y\sqrt{\kappa_{\|}\phi}}{\rho g\alpha_{\|}\xi}\right)\left[\left(h - \dfrac{\tau_y\alpha_{\|}\sqrt{\kappa_{\|}}}{\rho g\sqrt{\kappa_{\|}}\xi - \sqrt{\phi}\tau_y}\right) - \sqrt{\kappa_{\|}}\tanh\left(\dfrac{h_c(h,\xi)}{\sqrt{\kappa_{\|}}}\right)\right] \\ \qquad\qquad \text{when } h_c(h,\xi) > 0, \\ 0 \qquad\qquad \text{otherwise,} \end{cases}$$

and where

$$h_c(h,\xi) = \begin{cases} 0 & \text{when } h\left(\rho g\sqrt{\kappa_{\|}}\alpha_{\|}\xi - \sqrt{\phi}\tau_y\right) \leqslant \tau_y \\ G_{h,\xi}^{-1}(0) & \text{when } h\left(\rho g\sqrt{\kappa_{\|}}\alpha_{\|}\xi - \sqrt{\phi}\tau_y\right) > \tau_y \end{cases}$$

where forall $z \in]0,h]$ and $h,\ \xi$ in $\mathbb{R}^+$ the function G satisfies:

$$G_{h,\xi}(z) = \sqrt{\kappa_{\|}}\alpha_{\|}\tau_y\cosh\left(\frac{z}{\sqrt{\kappa_{\|}}}\right) + (z-h)\left(\sqrt{\kappa_{\|}}\alpha_{\|}\rho g\xi - \sqrt{\phi}\tau_y\right).$$

The equation (47) is completed by the boundary condition:

$$\frac{\partial(f+h)}{\partial n} = 0 \text{ on }]0,+\infty[\times\partial\Omega$$

and the initial condition:

$$h(t{=}0) = h_{\text{init}} \text{ in } \Omega.$$

The others unknowns p, $\mathbf{u}$, $\boldsymbol{\tau}$ and $\mathbf{f}_p$ can be explicitly expressed from h. The pressure directly expresses from h from the equation (22):

$$p(t,x,y,z) = \rho g\left(f(x,y) + h(t,x,y) - z\right).$$

Likewise, from (40), the horizontal velocity $\mathbf{u}_\parallel = (u_x, u_y)$ writes $\mathbf{u}_\parallel = -g(z)\boldsymbol{\nabla}_\parallel(f+h)$ with:

$$g(z) = \begin{cases} \dfrac{\rho g}{\eta}\left(\dfrac{\tau_y\sqrt{\kappa_\parallel\phi}}{\rho g\alpha_\parallel\xi} - \kappa_\parallel\right)\left(\dfrac{\cosh\left(\dfrac{f+h_c-z}{\sqrt{\kappa_\parallel}}\right)}{\cosh\left(\dfrac{h_c}{\sqrt{\kappa_\parallel}}\right)} - 1\right) & \text{when } z\in[f,f+h_c], \\ \dfrac{\rho g}{\eta}\left(\dfrac{\tau_y\sqrt{\kappa_\parallel\phi}}{\rho g\alpha_\parallel\xi} - \kappa_\parallel\right)\left(\dfrac{1-\cosh\left(\dfrac{h_c}{\sqrt{\kappa_\parallel}}\right)}{\cosh\left(\dfrac{h_c}{\sqrt{\kappa_\parallel}}\right)}\right) & \text{when } z\in\,]f+h_c,f+h]. \end{cases}$$

From (42) and the previous expression of $\mathbf{u}_\parallel$, the vertical velocity can be computed as:

$$u_z = w_e - \operatorname{div}_\parallel\left(\int_f^z \mathbf{u}_\parallel\,\mathrm{d}z\right).$$

From (16) and the previous expressions of $\mathbf{u}_\parallel$ and u_z, the components of the tensor $\boldsymbol{\tau}$ write:

$$\begin{aligned} \tau_{\alpha z} &= \left[\frac{\tau_y}{|\partial_z\mathbf{u}_\parallel|} + \eta\right]\partial_z u_\alpha, \quad \forall\alpha\in\{x,y\}, \\ \tau_{\alpha\beta} &= \left[\frac{\tau_y}{|\partial_z\mathbf{u}_\parallel|} + \eta\right]\left(\partial_\beta u_\alpha + \partial_\alpha u_\beta\right), \quad \forall\alpha,\beta\in\{x,y\}, \\ \tau_{zz} &= 2\left[\frac{\tau_y}{|\partial_z\mathbf{u}_\parallel|} + \eta\right]\partial_z u_z, \end{aligned}$$

when $z\in[f,f+h_c]$ and

$$|\boldsymbol{\tau}_\parallel| \leqslant \tau_y, \quad \text{otherwise.}$$

Finally, from (17), the Darcy's force writes:

$$\mathbf{f}_{p,\|} = -\left(\frac{\tau_y\sqrt{\kappa_\|\phi}}{\kappa_\|\alpha_\|\left|\mathbf{u}_\|\right|} + \frac{\eta}{\kappa_\|}\right)\mathbf{u}_\|,$$

for the horizontal components and

$$\mathbf{f}_{p,z} = -\left(\frac{\tau_y\sqrt{\kappa_\|\phi}}{\kappa_\perp\alpha_\|\left|\mathbf{u}_\|\right|} + \frac{\eta}{\kappa_\perp}\right)u_z,$$

for the vertical component, when $h_c > 0$, and

$$\left|\mathbf{f}_{p,\|}\right| \leqslant \frac{\tau_y\sqrt{\kappa_\|\phi}}{\kappa_\|\alpha_\|} \text{ when } h_c = 0.$$

3 Numerical method

3.1 A new dimensionless formulation

The nonlinear parabolic problem is first discretized in time by a full implicit second order variable step scheme. At each time-step, the subproblem is linearized by a Newthon algorithm. The resulting subproblems are discretized in space by a finite element method. From a computational point of view, it is convenient to consider a new dimensionless formulation. This second dimensionless procedure differs from the previous one as ε does no more appears in the zeroth order problem: the new dimensionless quantities are denoted with an hat. Let H be a characteristic length of the problem and let:

$$\hat{h} = \frac{h}{H},\ \hat{x} = \frac{x}{H},\ \hat{y} = \frac{y}{H},\ \hat{z} = \frac{z}{H},\ \hat{t} = \frac{t}{T},\ \hat{f} = \frac{f}{H},\ \widehat{w}_e = \frac{w_e}{U}$$

where $T = \dfrac{\eta}{\rho g H}$ represents a characteristic time and $U = \dfrac{\rho g H^2}{\eta}$ a characteristic velocity. After variable substitution, we obtain the following zeroth order dimensionless equation:

$$\partial_{\hat{t}}\hat{h} - \widehat{\mathrm{div}}_\|\left\{\hat{\mu}\left(\hat{h},\left|\widehat{\boldsymbol{\nabla}}_\|(\hat{f}+\hat{h})\right|\right)\ \widehat{\boldsymbol{\nabla}}_\|(\hat{f}+\hat{h})\right\} = \widehat{w}_e \ \text{ in }]0,+\infty[\times\widehat{\Omega}$$

where $\hat{\mu}$ is given by (44) by replacing $Da_\|$, Bi and $Bi_{p,\|}$ by the following new dimensionless numbers:

$$\widehat{Da}_\| = \frac{\kappa_\|}{H^2},\ \widehat{Bi} = \frac{\tau_y}{\rho g H},\ \widehat{Bi}_{p,\|} = \frac{\sqrt{\kappa_\|\phi}}{H\alpha_\|}\widehat{Bi}.$$

As we now only consider this dimensionless problem, and since there is no ambiguity, we omit the hat for all the quantities and also for the dimensionless numbers.

3.2 A second order implicit time scheme

Let $(t_m)_{m\geqslant 0}$ the discrete times and $\Delta t_m = t_{m+1} - t_m,\ m \geqslant 0$ the corresponding time steps. As the observed solutions decrease exponentially to an arrested state, we choose a geometric progression for the time step $\Delta t_{m+1} = \theta \Delta t_m$ where $\theta > 1$ and Δt_0 are given.

The time derivative is approximated by the following backward second order variable step finite difference scheme (BDF2), defined for all $\varphi \in C^0$ by:

$$\frac{\partial \varphi}{\partial t}(t_{m+1}) = \frac{2\Delta t_m + \Delta t_{m-1}}{\Delta t_m(\Delta t_m + \Delta t_{m-1})}\varphi(t_{m+1}) - \frac{\Delta t_m + \Delta t_{m-1}}{\Delta t_m \Delta t_{m-1}}\varphi(t_m)$$

$$+\frac{\Delta t_m}{(\Delta t_m + \Delta t_{m-1})\Delta t_{m-1}}\varphi(t_{m-1}) + \mathcal{O}(\Delta t_m^2 + \Delta t_{m-1}^2).$$

The approximate solution sequence $(h_m)_{m\geqslant 0}$, $h_m \approx h(t_m)$, is defined recursively, for all $m \geqslant 1$ by:

$(P)_m$: *h^{m-1} and h^m being known, find h^{m+1} such that:*

$$\alpha_m h^{m+1} - \mathrm{div}_{\|}\left\{\mu\left(h^{m+1},\ \left|\boldsymbol{\nabla}_{\|}(f + h^{m+1})\right|\right)\boldsymbol{\nabla}_{\|}(f + h^{m+1})\right\} = g_m + w_e \ \text{ in } \Omega \tag{48a}$$

$$\frac{\partial (f + h^{m+1})}{\partial n} = 0 \ \text{ on } \partial\Omega \tag{48b}$$

where

$$\alpha_m = \frac{2\Delta t_m + \Delta t_{m-1}}{\Delta t_m(\Delta t_m + \Delta t_{m-1})}$$

$$g_m = \frac{\Delta t_m + \Delta t_{m-1}}{\Delta t_m \Delta t_{m-1}}h^m - \frac{\Delta t_m}{(\Delta t_m + \Delta t_{m-1})\Delta t_{m-1}}h^{m-1}$$

The sequence is initiated by $h^{-1} = h^0 = h_{\text{init}}$ for $m = -1$ and 0, respectively and stopped when $||(\frac{\partial h}{\partial t})_m||_{L^2} < \epsilon$ where $(\frac{\partial h}{\partial t})_m$ is the approximation by means of the BDF2 scheme of $\frac{\partial h}{\partial t}(t_m)$ and ϵ is a tolerance that we fixe at 10^{-12} for all our simulations.

3.3 Newton algorithm

The initial time-dependent nonlinear parabolic problem is transformed as a sequence of nonlinear subproblems. It proposed in [5] an under-relaxed fixed point algorithm. We present here a new more efficiently Newton algorithm.

Define for all $m \geqslant 0$ and for all $h \in \mathbb{R}^+$ the function F_m:

$$F_m(h) = \alpha_m h - \mathrm{div}\left(\mu\left(h, \left|\boldsymbol{\nabla}_{\|}(f + h)\right|\right)\boldsymbol{\nabla}_{\|}(f + h)\right) - (g_m + w_e).$$

The problem (48) can be equivalently reformulate by using the function F_m:

$(P)_m$: *h^{m-1} and h^m being known, find h^{m+1} such that:*

$$\begin{aligned} F_m(h_{m+1}) &= 0, \quad \text{dans } \Omega, \\ \frac{\partial(f+h_{m+1})}{\partial n} &= 0, \quad \text{sur } \partial\Omega. \end{aligned}$$

The Newton algorithm writes:

Algorithm 1 (Newton)**.**

- $k=0 : \varphi^{(0)} := h_m$.
- $k \geqslant 1 :$ $\varphi^{(k)}$ known, find $\delta\varphi^{(k)}$ such that:

$$F'_m\left(\varphi^{(k)}\right)\delta\varphi^{(k)} = -F_m\left(\varphi^{(k)}\right),$$

- calculate explicitly:

$$\varphi^{(k+1)} := \varphi^{(k)} + \delta\varphi^{(k)},$$

where F'_m denotes the Fréchet derivative of F_m.

Note $\psi : \mathbb{R} \longrightarrow \mathbb{R}^2;\ h \mapsto \left(h, \left|\boldsymbol{\nabla}_{\|}(f+h)\right|\right)$ and $\zeta : \mathbb{R} \longrightarrow \mathbb{R};\ h \mapsto \mu \circ \psi(h)$. With these notations, $F_m(h) = \alpha_m h - \operatorname{div}\left(\zeta(h)\right)\boldsymbol{\nabla}_{\|}(f+h)) - (g_m + w_e)$. Start by calculate the Fréchet derivative of ζ. For all $h \in \mathbb{R}^+,\ \delta h \in \mathbb{R}^+ :\ \psi'(h)(\delta h) = \left(\delta h, \dfrac{\boldsymbol{\nabla}_{\|}(f+h).\boldsymbol{\nabla}_{\|}(\delta h)}{\left|\boldsymbol{\nabla}_{\|}(f+h)\right|}\right)$. Likewise, for all $h \in \mathbb{R}^+,\ \xi \in \mathbb{R}^+ :\ \boldsymbol{\delta Z} \in (\mathbb{R}^+)^2,\ \mu'(h,\xi)(\boldsymbol{\delta Z}) = \boldsymbol{\nabla}\mu(h,\xi).\boldsymbol{\delta Z}$. Finally, according to the rules of the derivative of the composition of functions:

$$\begin{aligned} \zeta'(h)(\delta h) &= \mu'(h,\xi) \circ \psi'(h)(\delta h) \\ &= \boldsymbol{\nabla}\mu(h,\xi).\left(\delta h, \frac{\boldsymbol{\nabla}_{\|}(f+h).\boldsymbol{\nabla}_{\|}(\delta h)}{\left|\boldsymbol{\nabla}_{\|}(f+h)\right|}\right), \end{aligned}$$

with $\boldsymbol{\nabla}\mu(h,\xi) = \left(\dfrac{\partial\mu}{\partial h}, \dfrac{\partial\mu}{\partial\xi}\right)(h,\xi)$ where

$$\begin{aligned} \frac{\partial\mu}{\partial h}(h,\xi) &= \left(Da_{\|} - \frac{Bi_{p,\|}}{\xi}\right)\left(1 - \frac{\partial h_c}{\partial h}(h,\xi)\frac{1}{\cosh^2\left(Da_{\|}^{-1/2}h_c\right)}\right), \\ \frac{\partial\mu}{\partial\xi}(h,\xi) &= \left(Da_{\|} - \frac{Bi_{p,\|}}{\xi}\right)\left(\frac{Bi}{(\xi - Da_{\|}^{-1}Bi_{p,\|})^2} - \frac{\partial h_c}{\partial\xi}(h,\xi)\frac{1}{\cosh^2\left(Da_{\|}^{-1/2}h_c\right)}\right) \\ &\quad + \frac{Bi_{p,\|}}{\xi^2}\left(\left(h - \frac{Bi}{\xi - Da_{\|}^{-1}Bi_{p,\|}}\right) - Da_{\|}^{1/2}\tanh\left(Da_{\|}^{-1/2}h_c\right)\right). \end{aligned}$$

The partial derivatives of h_c are obtained from the relation on h_c (37):

$$\begin{aligned}
\frac{\partial h_c}{\partial h} &= \frac{\xi - Da_{\|}^{-1} Bi_{p,\|}}{Da_{\|}^{-1/2} Bi \sinh\left(Da_{\|}^{-1/2} h_c\right) + \xi - Da_{\|}^{-1} Bi_{p,\|}} \\
&= \frac{1}{Da_{\|}^{-1/2} \tanh\left(Da_{\|}^{-1/2} h_c\right)(h - h_c) + 1}, \\
\frac{\partial h_c}{\partial \xi} &= \frac{h - h_c}{Da_{\|}^{-1/2} Bi \sinh\left(Da_{\|}^{-1/2} h_c\right) + \xi - Da_{\|}^{-1} Bi_{p,\|}} \\
&= \frac{h - h_c}{\left(\xi - Da_{\|}^{-1} Bi_{p,\|}\right)\left(Da_{\|}^{-1/2} \tanh\left(Da_{\|}^{-1/2} h_c\right)(h - h_c) + 1\right)}.
\end{aligned}$$

Finally, by using these partial derivatives and the relation (37) once again:

$$\begin{aligned}
\frac{\partial \mu}{\partial h}(h, \xi) &= \left(Da_{\|} - \frac{Bi_{p,\|}}{\xi}\right) \frac{Da_{\|}^{-1/2} \tanh\left(Da_{\|}^{-1/2} h_c\right)(h - h_c) + \tanh^2\left(Da_{\|}^{-1/2} h_c\right)}{Da_{\|}^{-1/2} \tanh\left(Da_{\|}^{-1/2} h_c\right)(h - h_c) + 1}, \\
\frac{\partial \mu}{\partial \xi}(h, \xi) &= \frac{Da_{\|}(h - h_c)}{\xi} \frac{Da_{\|}^{-1/2} \tanh\left(Da_{\|}^{-1/2} h_c\right)(h - h_c) + \tanh^2\left(Da_{\|}^{-1/2} h_c\right)}{Da_{\|}^{-1/2} \tanh\left(Da_{\|}^{-1/2} h_c\right)(h - h_c) + 1} \\
&\quad + \frac{Bi_{p,\|}}{\xi^2}\left(\left(h - \frac{Bi}{\xi - Da_{\|}^{-1} Bi_{p,\|}}\right) - Da_{\|}^{1/2} \tanh\left(Da_{\|}^{-1/2} h_c\right)\right).
\end{aligned}$$

Write now the explicit strong formulation of the linear tangent problem (LT):

■ (LT) *Let φ know, find $\delta\varphi$ defined on Ω such that*

$$\begin{aligned}
&\alpha_m \delta\varphi - \operatorname{div}\Bigg(\mu\left(\varphi, \left|\boldsymbol{\nabla}_{\|}(f + \varphi)\right|\right) \boldsymbol{\nabla}_{\|}\delta\varphi + \frac{\partial \mu}{\partial h}\left(\varphi, \left|\boldsymbol{\nabla}_{\|}(f + \varphi)\right|\right) \delta\varphi \boldsymbol{\nabla}_{\|}(f + \varphi) \\
&\qquad + \frac{\partial \mu}{\partial \xi}\left(\varphi, \left|\boldsymbol{\nabla}_{\|}(f + \varphi)\right|\right) \frac{\boldsymbol{\nabla}_{\|}(f + \varphi) \cdot \boldsymbol{\nabla}_{\|}\delta\varphi}{\left|\boldsymbol{\nabla}_{\|}(f + \varphi)\right|} \boldsymbol{\nabla}_{\|}(f + \varphi)\Bigg) = -F_m\left(\varphi^{(k)}\right) \\
&\qquad \frac{\partial(f + \delta\varphi)}{\partial n} = 0 \text{ on } \partial\Omega.
\end{aligned}$$

This linear subproblem is completely standard and is efficiently solved by a piecewise quadratic finite element method, as provided by the Rheolef library [33]. The numerical solution is obtained by solving the linear tangent problem in this weak form (WLT):

■ (WLT) *find $\delta\varphi \in W^{1,\infty}(\Omega)$ such that:*

$$a_1(\varphi; \delta\varphi, \delta\chi) = l_1(\delta\chi), \quad \forall \delta\chi \in W^{1,\infty}(\Omega),$$

where $a_1(.;.,.)$ and $l_1(.)$ are defined for all $\varphi, \delta\varphi, \delta\chi$ in $W^{1,\infty}(\Omega)$ by:

$$
\begin{aligned}
a_1(\varphi;\delta\varphi,\delta\chi) = \int_\Omega \Big(& \alpha_m \delta\varphi\delta\chi + \mu\left(\varphi, \left|\boldsymbol{\nabla}_\parallel(f+\varphi)\right|\right)\boldsymbol{\nabla}_\parallel\delta\varphi\cdot\boldsymbol{\nabla}_\parallel\delta\chi \\
& + \frac{\partial\mu}{\partial h}\left(\varphi, \left|\boldsymbol{\nabla}_\parallel(f+\varphi)\right|\right)\delta\varphi\boldsymbol{\nabla}_\parallel(f+\varphi)\cdot\boldsymbol{\nabla}_\parallel\delta\chi \\
& + \frac{\partial\mu}{\partial\xi}\left(\varphi, \left|\boldsymbol{\nabla}_\parallel(f+\varphi)\right|\right)\frac{1}{\left|\boldsymbol{\nabla}_\parallel(f+\varphi)\right|}(\boldsymbol{\nabla}_\parallel(f+\varphi)\cdot\boldsymbol{\nabla}_\parallel\delta\varphi)(\boldsymbol{\nabla}_\parallel(f+\varphi)\cdot\boldsymbol{\nabla}_\parallel\delta\chi)\Big)\,\mathrm{d}x, \\
l_1(\delta\chi) = & -\int_\Omega r\delta\chi\,\mathrm{d}x.
\end{aligned}
$$

Note, for all $\varphi \in \mathbb{R}^+$ and $\boldsymbol{\xi} \in \mathbb{R}^2$:

$$
\begin{aligned}
\boldsymbol{\beta}(\varphi,\boldsymbol{\xi}) &= \frac{\partial\mu}{\partial h}(\varphi,|\boldsymbol{\xi}|)\boldsymbol{\xi}, \\
k(\varphi,\boldsymbol{\xi}) &= \Big(\mu(\varphi,|\boldsymbol{\xi}|)\mathbf{I}_2 + \frac{\partial\mu}{\partial\xi}(\varphi,|\boldsymbol{\xi}|)\frac{1}{|\boldsymbol{\xi}|}\boldsymbol{\xi}\otimes\boldsymbol{\xi}\Big),
\end{aligned}
$$

where $\mathbf{I}_2$ is the identity matrix 2×2. Thus a_1 can be written with a more compact form:

$$
a_1(\varphi;\delta\varphi,\delta\chi) = \int_\Omega \alpha_m\delta\varphi\delta\chi + \Big(\delta\varphi\boldsymbol{\beta}\left(\varphi,\boldsymbol{\nabla}_\parallel(f+\varphi)\right) + k(\varphi,\boldsymbol{\nabla}_\parallel(f+\varphi))\boldsymbol{\nabla}_\parallel\delta\varphi\Big)\cdot\boldsymbol{\nabla}_\parallel\delta\chi\,\mathrm{d}x.
$$

4 Results and discussion

4.1 Comparison with the Vasilic's experiment [39]

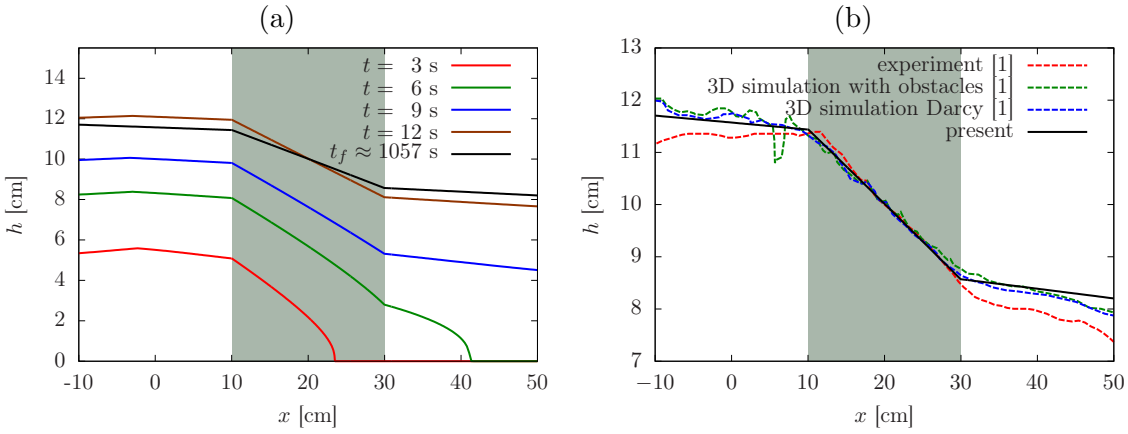

Figure 2: Views of the flow height along the container: (a) Flow heights at different times t = 3 s, 6 s, 9 s, 12 s and the final time $t_f \approx 1057$ s (obtained from BDF2 algorithm and the stopping condition); (b) comparison of the final height between present model and both observations and 3D simulations from [39]. The grey band represent the porous zone.

The Vasilic's experiment results are taken from [39]. During the experiment, 12 liters of Carbopol gel are slowly poured into a 20 x 20 x 60 cm transparent container. An array of $d = 3$ mm cylindrical steel bars is located in the middle zone and spaced of 19 mm in the two horizontal directions. The yield stress of this material was measured to be 15 Pa, while its plastic viscosity was measured to be around 1 Pa·s. The obtained value for the horizontal permeability components is $\kappa_{\|} = 6.34 \cdot 10^{-5}$ m^2 and $\alpha_{\|} = 1.5$ for the horizontal shift factor. The material flow through the funnel is replaced is our simulations by an equivalent injection. The total volume is injected with a supply rate of Q during a time t_e by means of an imposed vertical speed w_e through a vent. Assumme a circular vent with radius r_e cm center at the origin and a second order polynomial speed w_e versus the radius in the vent which writes:

$$w_e(t,r) = \begin{cases} \dfrac{2Q}{\pi r_e^4}(r_e^2 - r^2)^+ & \text{if } t \leqslant t_e, \\ 0 & \text{if } t > t_e. \end{cases} \tag{50}$$

The values used in simulations are $Q = 1$ l/s, $r_e = 5$ cm and $t_e = 12$ s.

Fig. 2 (a) shows the shape of the flow at different times. Observe that the porous zone has an effect on the spreading. After 12 s, the flow is not anymore supplied, it is slowly still moving until the stoppage. Fig. 2 (b) compares our results with both laboratory experiments and 3D simulations from [39], using a regularized Bingham model. Results are shown at the final arrested state. Notice that, neglecting lateral wall effects, our problem here still reduces to a 1D time dependent one. Observe good quantitative agreement of the present approach with both experimental observations and 3D simulations, especially for the slop of the flow front within the porous zone. The discrepancies that can be observed before and after the porous zone, might be result of wall effect during the experiment.

4.2 Flow on a sloped plan for different porous mediums characteristics

We present here results for a new numerical experiment. Differents simulations have been made for a flow injected on an inclined plan and which crossing a porous zone. The rheological parameters used are $\eta = 1$ Pa·s and $\tau_y = 20$ Pa. Two angles of inclinaison have been employed: $\theta = 5°$ and $\theta = 10°$. Differents porous medium configurations have been investigated. Their characteristics have been defined from different geometrical configurations of periodic array of vertical cylinders. By noting d the diameter of the cylinders, M the distance which them separates and $X = M/d$ the relative distance, the porosity value is $\phi = 1 - a/(1+X)^2$ where a is the fiber arrangement, $a = \pi/4$ for square packing and $a = \pi/(2\sqrt{3})$ for hexagonal packing. The permeability can be computed by numerical simulation using Newtonian fluid as proposed in [40] or approximated by a formula like the law of Tamayol and Bahrami [38] where the horizontal permeability is a function of the porosity and the fiber arrangement:

$$\kappa_{\|}(\phi) = d^2\ 0.16\ a\frac{\left(1-\sqrt{(1-\phi)/a}\right)^3}{(1-\phi)\sqrt{\phi}}.$$

The simulations have been realised for a square packing ($a = \pi/4$) of $d = 3$ mm cylinders. The total injected volume is 6 liters by means of an imposed vertical speed w_e following the law (50) shown in the previous section with a supply rate of $Q = 1$ l/s, a vent radius $r_e = 5$ cm and an injection duration $t_e = 6$ s.

The Fig. 3 gives a qualitative comparison of the final state after the stoppage for two simulations, with an angle of $\theta = 5°$ and in (a) without porous zone (denoted by the label $X = \infty$) and in (b) with $X = 6$. The permeability is calculated by the Tamayol and Bahrami's law. We clearly observe that the presence of a porous zone change completely the shape of the flow.

(a) $X = \infty$ (b) $X = 6$

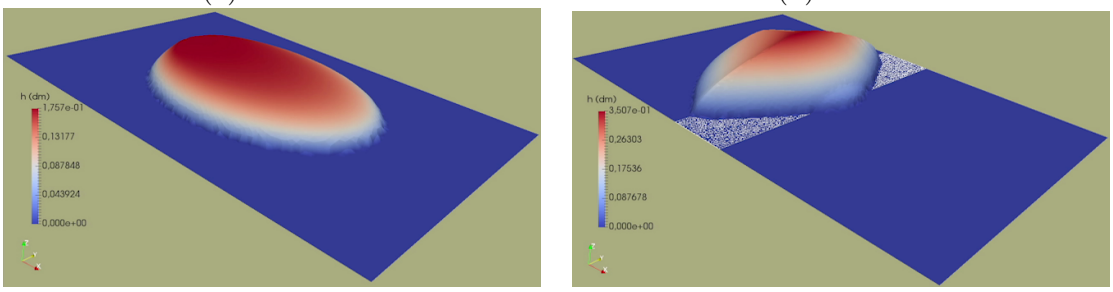

Figure 3: Comparative 3D views for $\theta = 5°$ and (a) $X = \infty$ (without obstacles) and (b) $X = 6$. The white zone on (b) represents the porous zone.

For a more quantitative comparison, the final height along the symmetry line and the final front contours for a range of relative distances X are shown on the Fig. 4. We observe on Fig. 4 that more the distance between obstacle is high, more the flow is close to the case without obstacles ($X = \infty$). When the distance decreases, we observe by the front views on Fig. 4 (a) and (b) that the flow spreads more laterally and less in the slop direction. Observe on 4 (c) and (d) that a higher thickness of fluid piles up in the porous zone. We can conclude from the Fig. 4 that the presence of a porous zone has a limiting effect on the spatial flow propagation by widening the spreading on the lateral sides and by accumulating more volume of fluids per unit surface.

The Fig. 5 shows the maximum flow advance $x_{\max}(t)$ in the slop direction versus real physical time for several relative distances X. We observe that the presence of porous zone has also an delaying effect by slowing the flow in the slop direction.

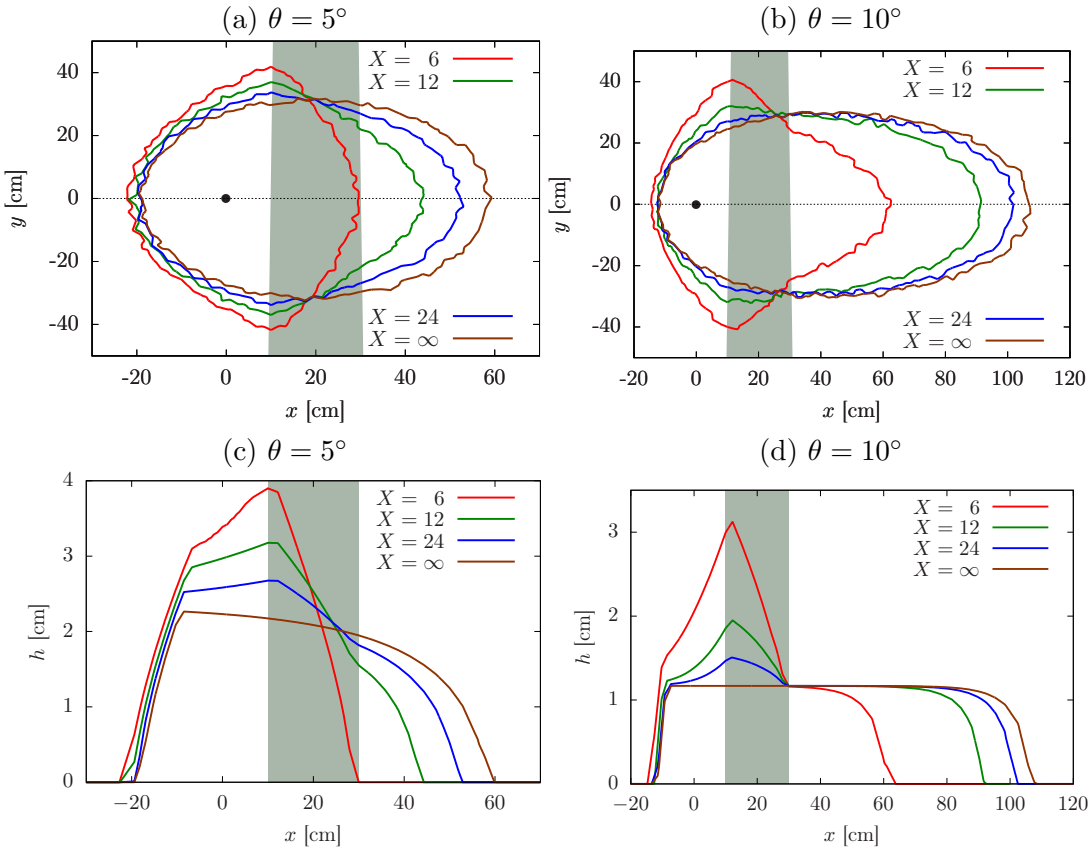

Figure 4: Comparative views for different relatives distances between obstacles $X = 6, 12, 24, \infty$ of the final front contours in (a) for $\theta = 5°$ and in (b) for $\theta = 10°$ and the final heights along the symmetry line in (c) for $\theta = 5°$ and in (d) for $\theta = 10°$. The grey band represent the porous zone and the dot «•» the center of the injection.

5 Conclusion

A new reduced model has been developed for laminar shallow viscoplastic fluids flowing on a general topography and crossing an array of vertical obstacles. The model includes two mathematical reductions. The first reduction replaces the obstacles zone by a fibrous media using an extended tensor form of the Brinkman equations for the Bingham rheological behaviour. The second reduction in the vertical direction bases on an asymptotic analysis based on the shallow-depth approximation. An efficient numerical resolution using the BDF2 algorithm for time-discretization and a Newton algorithm for nonlinearities have been developed in Section 3. The sequence of linear subproblems are solved by a finite element method. Finally, two numerical applications are detailed. A comparison with the measurements and 3D-simulations of [39] shows that the present results are in a good quantitative agreement. The advantage with the present reduced model is that the computational-time took few minutes for simulations instead a few hours for 3D-simulations from [39]. We propose also a numerical benchmark concerning the flow of a Bingham fluid over an inclined plane which pass through a fibrous media. The simulations

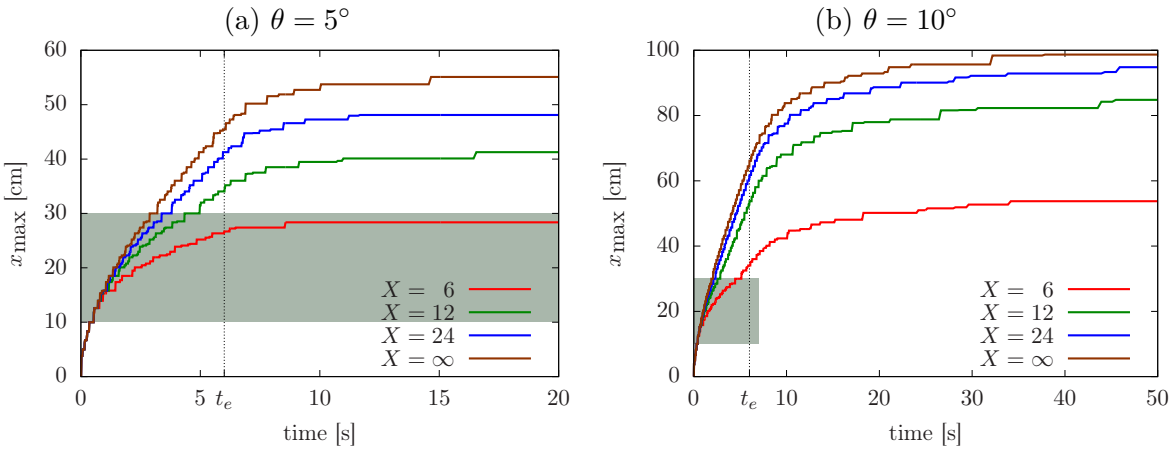

Figure 5: Evolution in time of the maximum flow advance for several relative distances $X = 6, 12, 24, \infty$ with a slop $\theta = 5°$ in (a) and $\theta = 10°$ in (b). The grey band shows the passage of the front into the porous zone. The supply duration is $t_e = 6$ s.

produced for a range of obstacle densities showed the ability of a porous zone to limit the spatial flow advance and to delay it. This suggests to reproduce this study experimentally and compare with the present results. Other further work would be to extend the asymptotic analysis presented here for Bingham material to Herschel-Bulkley one. For natural applications such as volcanic lava flows through forest, perspectives will be to include complex topographies and thermal effects as developed before in [6] and to integrate new thermal effects specific to the trees burning. In this regard, volcanoes are often vegetated, and ingress of lava into such zones will dry, ignite and burn vegetation, and can encase trees in lava to create vertically-oriented solid objects known as "lava trees" [17, 26].

References

[1] T. Al-Fariss and K. L. Pinder. Flow through porous media of a shear-thinning liquid with yield stress. *Canadian J. Chem. Eng.*, 65(3):391–405, 1987.

[2] D. Andronico, S. Branca, S. Calvari, M. Burton, T. Caltabiano, R. A. Corsaro, P. Del Carlo, G. Garfì, L. Lodato, L. Miraglia, F. Murè, M. Neri, E. Pecora, M. Pompilio, G. Salerno, and L. Spampinato. A multi-disciplinary study of the 2002–03 etna eruption: insights into a complex plumbing system. *Bulletin of Volcanology*, 67(4):314–330, 2005.

[3] N. J. Balmforth, A. S. Burbidge, R. V. Craster, J. Salzig, and A. Shen. Visco-plastic models of isothermal lava domes. *J. Fluid Mech.*, 403:37–65, 2000.

[4] N. J. Balmforth and R. V. Craster. A consistent thin-layer theory for Bingham plastics. *J. Non-Newt. Fluid Mech.*, 84(1):65–81, 1999.

[5] N. Bernabeu, P. Saramito, and C. Smutek. Numerical modeling of shallow non-Newtonian flows: Part II. Viscoplastic fluids and general tridimensional topographies. *Int. J. Numer. Anal. Model.*, 11(1):213–228, 2014.

[6] N. Bernabeu, P. Saramito, and C. Smutek. *Modelling lava flow advance using a shallow-depth approximation for three-dimensional cooling of viscoplastic flows*, chapter 27. Geol. Soc., London, 2016.

[7] E. C. Bingham. *Fluidity and plasticity.* Mc Graw-Hill, New-York, USA, 1922.

[8] J. Bleyer and P. Coussot. Breakage of non-Newtonian character in flow through a porous medium: evidence from numerical simulation. *Phys. Rev. E*, 89(6):063018, 2014.

[9] F. Bouchut, A. Mangeney-Castelnau, B. Perthame, and J.-P. Vilotte. A new model of saint venant and savage–hutter type for gravity driven shallow water flows. *C. R. Math.*, 336(6):531–536, 2003.

[10] A. Bourgeat and A. Mikelić. Homogenization of a polymer flow through a porous medium. *Nonlin. Anal. Theory Meth. Appl.*, 26(7):1221–1253, 1996.

[11] D. Bresch, E. D. Fernández-Nieto, I. R. Ionescu, and P. Vigneaux. Augmented lagrangian method and compressible visco-plastic flows: applications to shallow dense avalanches. In *New directions in mathematical fluid mechanics*, pages 57–89. Springer, 2009.

[12] H. C. Brinkman. A calculation of the viscous force exerted by a flowing fluid on a dense swarm of particles. *Appl. Sci. Res.*, 34:27–34, 1947.

[13] T. Chevalier, C. Chevalier, X. Clain, J. C. Dupla, J. Canou, S. Rodts, and P. Coussot. Darcy's law for yield stress fluid flowing through a porous medium. *J. Non-Newt. Fluid Mech.*, 195:57–66, 2013.

[14] H. P. G. Darcy. *Détermination des lois d'écoulement de l'eau à travers le sable*, chapter Annexe D, pages 559–603. V. Dalmont, éditeur, Paris, 1856. http://gallica.bnf.fr/ark:/12148/bpt6k624312.

[15] E. D. Fernández-Nieto, J. M. Gallardo, and P. Vigneaux. Efficient numerical schemes for viscoplastic avalanches. Part 2: the 2D case. *J. Comput. Phys.*, 353:460–490, 2018.

[16] E. D. Fernández-Nieto, P. Noble, and J.-P. Vila. Shallow water equations for power law and bingham fluids. *Science China Mathematics*, 55(2):277–283, 2012.

[17] R. H. Finch. Lava tree casts and tree molds. *Volc Lett*, 316:1–3, 1931.

[18] A. Herault, A. Vicari, A. Ciraudo, and C. Del Negro. Forecasting lava flow hazards during the 2006 etna eruption: using the magflow cellular automata model. *Computers & Geosciences*, 35(5):1050–1060, 2009.

[19] D. R. Hewitt, M. Daneshi, N. J. Balmforth, and D. M. Martinez. Obstructed and channelized viscoplastic flow in a Hele-Shaw cell. *J. Fluid Mech.*, 790:173–204, 2016.

[20] G. Hulme. The interpretation of lava flow morphology. *Geophys. J. Int.*, 39(2):361–383, 1974.

[21] I. R. Ionescu. Onset and dynamic shallow flow of a viscoplastic fluid on a plane slope. *J. Non-Newt. Fluid Mech.*, 165(19):1328–1341, 2010.

[22] I. R. Ionescu. Augmented lagrangian for shallow viscoplastic flow with topography. *J. Comput. Phys.*, 242:544–560, 2013.

[23] D. Laigle and P. Coussot. Numerical modeling of mudflows. *J. Hydraulic Eng.*, 123(7):617–623, 1997.

[24] P. W. Lipman, J. P. Lockwood, R. T. Okamura, D. A. Swanson, and K. M. Yamashita. Ground deformation associated with the 1975 magnitude-7.2 earthquake and resulting changes in activity of kilauea volcano, hawaii. Technical report, US Government Printing Office, 1985.

[25] K. F. Liu and C. C. Mei. Approximation equations for the slow spreading of a thin Bingham plastic fluid. *Phys. Fluids A*, 2(1):30–36, 1990.

[26] J. P. Lockwood and I. S. Williams. Lava trees and tree moulds as indicators of lava flow direction. *Geological Magazine*, 115(1):69–74, 1978.

[27] S. P. Neuman. Theoretical derivation of darcy's law. *Acta Mech.*, 25(3):153–170, 1977.

[28] H. Pascal. Nonsteady flow through porous media in the presence of a threshold gradient. *Acta Mech.*, 39(3-4):207–224, 1981.

[29] J. R. A. Pearson and P. M. J. Tardy. Models for flow of non-newtonian and complex fluids through porous media. *Journal of Non-Newtonian Fluid Mechanics*, 102(2):447–473, 2002.

[30] M. Poreh and C. Elata. An analytical derivation of darcys law. In *Israel J. Tech.*, volume 4, page 214, 1966.

[31] D. Rickenmann, D. Laigle, B. W. McArdell, and J. Hübl. Comparison of 2D debris-flow simulation models with field events. *Comput. Geo.*, 10(2):241–264, 2006.

[32] A. Roustaei, T. Chevalier, L. Talon, and I. A. Frigaard. Non-darcy effects in fracture flows of a yield stress fluid. *J. Fluid Mech.*, 805:222–261, 2016.

[33] P. Saramito. *Efficient C++ finite element computing with Rheolef*. CNRS and LJK, 2015. https://www-ljk.imag.fr/membres/Pierre.Saramito/rheolef.

[34] P. Saramito. *Complex fluids: modelling and algorithms*. Springer, 2016.

[35] P. Saramito and A. Wachs. Progress in numerical simulation of yield stress fluid flows. *J. Rheol.*, 56(3):211–230, 2017.

[36] S. Shahsavari and G. H. McKinley. Mobility and pore-scale fluid dynamics of rate-dependent yield-stress fluids flowing through fibrous porous media. *J. Non-Newt. Fluid Mech.*, 235:76–82, 2016.

[37] K. S. Sorbie, P. J. Clifford, and E. R. W. Jones. The rheology of pseudoplastic fluids in porous media using network modeling. *J. Colloid Interface Sci.*, 130(2):508–534, 1989.

[38] A. Tamayol and M. Bahrami. Transverse permeability of fibrous porous media. *Phys. Rev. E*, 83(4):046314, 2011.

[39] K. Vasilic. *A numerical model for self-compacting concrete flow through reinforced sections: a porous medium analogy*. PhD thesis, faculty of civil engeenering, Dresden, Germany, 2016. https://opus4.kobv.de/opus4-bam/frontdoor/deliver/index/docId/35783/file/diss144_vt.pdf.

[40] K. Vasilic, B. Meng, H.-C. Kühne, and N. Roussel. Flow of fresh concrete through steel bars: a porous medium analogy. *Cement Concrete Res.*, 41(5):496–503, 2011.

[41] K. Vasilic, W. Schmidt, H.-C. Kühne, F. Haamkens, V. Mechtcherine, and N. Roussel. Flow of fresh concrete through reinforced elements: experimental validation of the porous analogy numerical method. *Cement Concrete Res.*, 88:1–6, 2016.